SAT-MAP-CLIMATE project results

Hasager, C.B.; Nielsen, N.W.; Soegaard, H.; Boegh, E.; Christensen, J.H.; Jensen, N.O.; Rasmussen, M.S.; Astrup, P.; Dellwik, E.

Publication date:
2002

Document Version
Publisher's PDF, also known as Version of record

Risø-R-1350(EN)

SAT-MAP-CLIMATE Project Results

Charlotte Bay Hasager, Niels Woetmann Nielsen, Henrik Soegaard, Eva Boegh, Jens Hesselbjerg Christensen, Niels Otto Jensen, Michael Schultz Rasmussen, Poul Astrup and Ebba Dellwik

Risø National Laboratory, Roskilde
August 2002

Abstract Earth Observation (EO) data from imaging satellites are analysed with respect to albedo, land and sea surface temperatures, land cover types and vegetation parameters such as the Normalized Difference Vegetation Index (NDVI) and the leaf area index (LAI). The observed parameters are used in the DMI-HIRLAM-D05 weather prediction model in order to improve the forecasting. The effect of introducing actual sea surface temperatures from NOAA AVHHR compared to climatological mean values, shows a more pronounced land-sea breeze effect which is also observable in field observations. The albedo maps from NOAA AVHRR are rather similar to the climatological mean values so for the HIRLAM model this is insignicant, yet most likely of some importance in the HIRHAM regional climate model. Land cover type maps are assigned local roughness values determined from meteorological field observations. Only maps with a spatial resolution around 25 m can adequately map the roughness variations of the typical patch size distribution in Denmark. A roughness map covering Denmark is aggregated (ie area-average non-linearly) by a microscale aggregation model that takes the non-linear turbulent responses of each roughness step change between patches in an arbitrary pattern into account. The effective roughnesses are calculated into a 15 km by 15 km grid for the HIRLAM model. The effect of hedgerows is included as an added roughness effect as a function of hedge density mapped from a digital vector map. Introducing the new effective roughness maps into the HIRLAM model appears to remedy on the seasonal wind speed bias over land and sea in spring. A new parameterisation on the effective roughness for scalar surface fluxes is developed and tested on synthetic data. Further is a method for the estimation the evapotranspiration from albedo, surface temperatures and NDVI succesfully compared to field observations. The HIRLAM predictions of water vapour at 12 GMT are used for atmospheric correction of the satellite parameters derived in the afternoon.

ISBN 87-550-3079-3
ISBN 87-550-3080-7 (Internet)
ISSN 0106-2840

Print: Pitney Bowes Management Services Denmark A/S, 2002

Contents

1 Introduction

The SAT-MAP-CLIMATE project is an acronym for the project

"SATellite based bio-geophysical parameter MAPping and aggregation modelling for CLIMATE models".

The project is carried out by three Danish partners

- Risø National Laboratory, Wind Energy Department, Atmospheric Physics Programme (RISØ)
  Charlotte Bay Hasager (PI), Niels Otto Jensen, Poul Astrup and Ebba Dellwik

- Danish Meteorological Institute, The Research Department and the Climate Center (DMI)
  Niels Woetmann Nielsen and Jens Hesselbjerg Christensen

- University of Copenhagen, Institute of Geography (IGUC)
  Henrik Soegaard, Eva Boegh and Michael Schultz Rasmussen

The project period is from April 1, 1999 to April 1, 2002.

Funding for the project is granted by the Danish Research Council, The ESA-foelgeforskning (Space Research) Grant, Sagsnr. 5006-00-0063.

1.1 Reporting

The report provides a detail description of the research and results obtained within the SAT-MAP-CLIMATE project. Other publications from the project are listed in Appendix I. Updated general information on the project and participant institutions is available at http://www.risoe.dk/vea-atu/SAT-MAP-CLIMATE/.

1.2 Workshop and conference activities

The scientific results are presented at many international workshops and conferences. This is to ensure a good interaction with the international scientific community and stimulate joint cooperation at an international level. A chronological list is given here from recent to first

- *34th COSPAR Assembly Scientific (Committee on Space Research) at the Second World Space Congress.* Houston, Texas, USA, 10-19 Oct 2002 (SOLICITED oral presentation, planned)

- *First International Symposium on Recent Advances in Quantitative Remote Sensing*, Valencia, Spain, 16-20 Sep 2002 (planned)

- *Nordic Meteorological Meeting (Nordisk Meteorolog Møde).* Copenhagen, Denmark, 27-31 May 2002

- *European Geophysical Society (EGS) 2002, 27. General Assembly,* Nice, France, 21-26 April 2002

- *HIRLAM ASM* Copenhagen, Denmark, 4 April 2002

- *American Geophysical Union (AGU) Fall Meeting*, San Francisco, CA, USA, 10-14 Dec 2001.

- *Danish Society on Atmospheric Research (DSAR) Annual Meeting*, Copenhagen (DK), 15 Nov 2001

- *International Workshop on Landscape Heterogeneity and Aerodynamic Roughness: Modelling and Remote Sensing Perspectives*, VITO, Antwerp, Belgium, 12 Oct. 2001 (INVITED*)

- *International Workshop on Remote Sensing in Hydrology,* Montpellier, France, 2-5 October 2001

- *International Geoscience and Remote Sensing Symposium IGARSS 2000 Symposium,* Honolulu, HI, USA, 24- 28 July 2000)

- *European Geophysical Society (EGS). 25. General Assembly: Millennium Conference on Earth, Planetary and Solar Systems Sciences,* Nice, France, 25-29 Apr 2000

- *International Symposium on Remote Sensing and Hydrology 2000*, Santa Fe, New Mexico, USA, 2-7 April 2000.

- *International Union of Geodesy and Geophysics, IUGG 99*, Birmingham, UK, 18-30 July 1999

* C.Hasager was invited speaker with all costs covered by VITO.

It was envisioned to have an international workshop in Denmark organized by the SAT-MAP-CLIMATE project. For econonical reasons this was not conducted.

1.3 Educational activities

Educational and research training includes that one graduate student, Rasmus Houborg has been involved in the project and is presently reporting his work in a M.Sc thesis at IGUC. Furthermore, one Ph.D. student, Ebba Dellwik at Risø, and one Post.Doc. fellow, Eva Boegh at IGUC, have benefited in educational terms from the scientific cooperation within the SAT-MAP-CLIMATE project.

2 Background

Global climate change is on the scientific agenda as well as the political, eg manifest in the Kyoto Protocol ratified in 1997 (IGBP 1998). The perception that we live in a "global village" most likely is based on the new travel patterns of mankind, our continuous access to global information and some physical understanding of air- and water pollution transcending national borders or even more fantastic "the stroke of a butterfly that may cause a gale on the other hemisphere" (Gleick 1987).

Global climate change is a complex issue in the sense that very many interactions are involved from the very small scale, eg plant physiological responses to changes in ambient CO_2 and temperature conditions, to the large scale climatic trends in precipitation patterns.

It is only possible to link all the bio-geophysical processes together through comprehensive mathematical models such as Soil-Vegetation-Atmosphere-Transfer (SVAT) models and Global Circulation Models (GCMs). The data that are fed into such models traditionally are sampled more or less continuously on the ground at selected locations.

Earth Observation (EO) data provide the spatial coverage of the state of the bio-geophysical nature of land and ocean. Some parameters are slowly changing, others very fast. However, it is only feasible to map the various parameters at certain points in time. EO data in most cases provide measures of bio-geophysical parameters somewhat different from traditional point data.

The limitations of EO data are that these are only available at a highly discontinuous basis (cloud cover being one reason) and that image data are not directly comparable to traditional ground data. The advantages of EO data are that these are area-averaged values of several important bio-geophysical parameters that can be retrieved such as vegetation state, surface temperature and surface roughness. These parameters relates directly to vegetation-atmosphere interactions and hence would be useful in large scale climate models after proper area-averaging (aggregation).

During the last decade a number of projects have shown how land surface properties can be derived from satellite data (Carlson et al. 1993, Kidder and Haar 1995, Stewart et al. 1996). At the same time high resolution meteorological models have proven their value in terms of weather forecasting. The inevitable coupling between land surface processes and meteorological processes has, however, only to a limited extent reached the operational models. In most climate models the parameterization of surface characteristics, eg the sensible and latent heat flux is still on a rather immature level. The aim for the present project is to overcome this threshold by re-parametrizing a number of important surface processes in a way so that they can be taken into account in meteorological models of the HIRLAM type (Sass 1994).

In the long run this might lead to better forecasts of weather and climate but on the short term meteorological models with an improved land surface description would be a strong tool for integration of remote sensing and traditional point observation into spatial distributed *surface flux climatology mapping*.

HIRLAM (High Resolution Limited Area Model) is a routine weather forecasting model used by DMI, FMI, IMS, KMNI, INM and SMHI (weather services in resepectively, Denmark, Finland, Ireland, The Netherlands, Spain and Sweden). The HIRLAM models used at DMI are three nested models (G45, E15 and D05) where G45 covers a sixth of the Northern Hemisphere, E15 covers Western Europe and the North Atlantic and D05 covers Denmark and interior seas (see Figure 7-1). The horizontal resolutions are 0.45°, 0.15° and 0.05° with integration timesteps of 240, 100 and 30 seconds, respectively. Each of the models have 31 atmospheric layers and 3 soil layers. G45 uses 12 hour old predictions from the European Centre for Medium Range Weather Forecasts model at the lateral boundaries, while E15 uses 0 hour old predictions from G45 and D05 0 hour old predictions from E15. G45 get lateral boundary conditions every 6 hours, E15 every 3 hours and D05 every 1 hour.

3 Goal and objectives

3.1 Goal

Integrate Earth Observation (EO) data as surface boundary conditions in the HIRLAM weather prediction model and the HIRHAM regional climate model for impact assessment of land surface processes to weather forecasting and climate prediction.

3.2 Objectives

- Satellite maps
  From atmospheric corrected satellite images derive high-resolution maps of bio-geophysical parameters of vegetation, surface temperature, albedo and roughness for Denmark.

- Aggregation
  Calculate area-averaged values of the surface boundary conditions from the satellite-based maps.

- Validation of HIRLAM weather forecasting
  Verification assessment of the improved surface boundary condition for weather forecasting.

- One-year impact study in HIRHAM regional climate model
  Implementation of area-averaged surface boundary conditions in the HIRHAM regional climate model for one-year impact studies.

4 Satellite maps

Satellite scenes are useful for mapping the areal distrubution of vegetation, surface temperature, albedo and surface roughness. A land cover mapping of Denmark will is produced from high- and low-resolution satellite scenes. The satellite mapping parameters includes

- land cover classification into roughness classes per season
- surface temperature for land and sea conditions at specific days
- global albedo
- vegetation conditions from NDVI
- vegetation state describing the Leaf Area Index (LAI)
- T_s-NDVI relationship for water vapour fluxes.

In order to establish time series of the global albedo and NDVI, atmospheric correction of the satellite data is required. For this purpose, the HIRLAM model provides the relevant meteorological data required by a radiative transfer model to facilitate the atmospheric correction of satellite imagery.

The availability of high-resolution scenes is very good. Landsat-7 TM is available since year 1999, ENVISAT from 2002 and QuickBird from 2001. Other current high-resolution satellites are Landsat-5, SPOT, IRS-1C LISS III and Resurs. The best available satellite scenes are chosen from cloud cover, time of the year and pricing, as to map regions in Denmark. National multi-daily coverage by NOAA AVHRR medium-resolution satellite scenes received at IGUC is also used. The use of ERS SAR is not implemented in this project because methods applied for SAR evaluation of aerodynamic roughness and soil moisture are not fully operational (Soegaard et al. 1998).

The satellite-based maps of vegetation and roughness are compared to other available sources of land surface parameters. The available maps at high resolution are investigated such as the CORINE (EEA, 1992) and Areal Information System (AIS) (Danish Areal Information System, 2001). Both these maps are based on Landsat TM scenes. The HIRLAM model is recently updated to cover up to 20 land surface classes (in contrast to previously only two, land, ice and sea). For the sea the roughness (z_0) is calculated from the wind field.

4.1 Albedo

All midday/afternoon NOAA AVHRR satellite passages in the year 1998 and in the period 15th April-15th May 2000 are downloaded from the NOAA HRPT receiving station facilities at the Institute of Geography, Copenhagen. The data set is cloud screened and images with extreme off-nadir view-angles are detached. The image processing is conducted using the software WinCHIPS (www.geogr.ku.dk/chips) which includes a NOAA module for unpacking, geo-registration, calibration and calculation of the spectral albedo.

The calculation of the spectral surface albedoes includes HIRLAM predictions of integrated atmospheric water vapour content to facilitate the atmospheric correction of the satellited data. Atmospheric correction of the data recorded by the AVHRR sensors onboard the NOAA satellites is conducted using the 5S radia-

tive transfer model (Tanré et al., 1987). Details on the processing is described in Boegh et al. (2002b).

Calculation of the global albedo is based on a conversion of the narrow-band red (0.57-0.7 μm) and near-infrared (0.72-0.99 μm) albedoes computed from the NOAA-AVHRR channels into a broad-band (0.3-2.5 μm) albedo. For this purpose, the method of Valiente et al. (1995) is used which is independent of the surface type. The spatial resolution of the global albedo is 1 km.

Time series of the AVHRR estimated global albedo are extracted for agricultural land (Foulum), a beech forest (the EUROFLUX[1] setup in Sorø) and a conifer forest (Ulborg site) for further analysis (chapter 5). In the agricultural region, the albedo increases from around 10 % in winter to around 18 % in summer. The global albedo for the beech forest reached its lowest level during spring (10 %) at the time where the beech comes into leaf and there is an abundance of forest floor vegetation. The average albedo of the beech forest during summer is 16.8 %. For the conifer forest, the global albedo is lower (10 %) due to the larger efficiency with which the needles capture light.

4.2 Sea and land surface temperatures

The AVHRR thermal channels (1 km spatial resolution) are converted to estimates of sea surface temperature using the "split window algorithm" which gives an estimate of the water surface (skin) temperature corrected for atmospheric effects with an accuracy of about 0.2 °C (Soegaard et al., 2002)

The calculation of land surface temperature uses a split window algorithm which is modified for land surface (Price, 1984). Considering the large difference in observation scales, the AVHRR land surface temperatures compared favourably with field measurements of surface temperature recorded for agricultural land and for a beech forest (Boegh et al., 2002b).

4.3 Land cover classification

For the microscale roughness aggregation study, a high-resolution land cover map is obtained by using Landsat TM (30 m resolution) and SPOT (20 m resolution) satellite data to classify the land surface into distinct surface types. The land cover classification is performed for the Foulum region in 1998 and 1999 by applying multi-temporal satellite information on spectral albedo and NDVI (section 4.4) in a minimum distance classifier (Boegh et al., 2000). The accuracies of the land cover maps are 86 % (1998) and 80 % (1999). In addition, the satellite based land cover maps provided by the Danish Areal Information System (AIS) (Danish Areal Information System, 2001) and CORINE (EEA, 1992) at spatial resolutions of 25 m and 250 m, respectively, were used to represent land cover classes at the national level. While the regional Foulum map has 9 agricultural classes, the maps at the national level have 1-2 agricultural classes. To facilitate a quantitative evaluation of the effect of spatial scale on the effective surface roughness, the classes were regrouped into simplified classes (chapter 6).

1 EUROFLUX, European Commission project, Year 1996- , European network on long-term CO_2 flux in forest. Part of FLUXNETglobal CO_2 monitoring. Now EU project CARBO-EUROFLUX, Http://www.unitas.it/eflux/euro.html

4.4 Vegetation and leaf area index

The AVHRR atmospheric corrected red and near-infrared albedoes are used for computing the Normalized Difference Vegetation Index (NDVI) which is strongly related to the green vegetation leaf area index (LAI).

The NDVI peaks during summer. For the EUROFLUX beech forest, the increase in NDVI during spring is more rapid than for the agricultural land (Foulum), while the decline during autumn is slower for the beech forest. The conifer (Ulborg) NDVI is relatively stable throughout the year (Boegh et al., 2002b).

4.5 Summary

Satellite data acquired from the NOAA-AVHRR sensor are atmospherically corrected using the meteorological data which are predicted by the HIRLAM model. The processed satellite data are used to establish temporal maps of the global albedo, NDVI, sea surface temperature and land surface temperature for Denmark in the year 1998 and during 1 month in year 2000 which is characterized by favourable weather conditions (clear sky). The extraction of time series of global albedo and NDVI for three field sites in Denmark (agriculture, beech forest and conifer) disclosed variations related to differences in vegetation characteristics and vegetation development rates. The sea and land surface temperatures compare favourably with field data.

Multi-resolution satelllite based land cover maps are acquired. A very detailed map is constructed using multi-temporal high-resolution (20-30 m) satellite data for the Foulum region. At the national level, the AIS (25 m) and CORINE (250 m) maps are used. The multi-resolution land cover maps are used in the micro-scale aggregation study of surface roughness (chapter 6).

5 Evapotranspiration modelling

The need for an accurate surface parameterization in large-scale atmospheric modelling and the requirement for meteorological data for the atmospheric correction of satellite data resolve a strong synergism between climate modelling and quantitative remote sensing based studies. While the satellite data can supply the model with a spatial describtion of relevant surface parameters, the climate model provides the meteorological data facilitating the atmospheric correction of satellite imagery.

This section summarizes results from the implementation of HIRLAM weather predictions in remote sensing based calculation of evapotranspiration rates in Denmark. At the national level, the retrieval of meteorological data may be cumbersome or expensive, and the lack of representative spatially distributed meteorological data may sincerely constraint the accuracy of remote sensing based flux estimation. Because the HIRLAM weather prediction model provides spatially distributed information on air temperature and air humidity of the lower atmospheric boundary level, weather predictions are particular valuable for remote sensing based flux estimation at larger scales.

5.1 Combining weather predictions and satellite data

HIRLAM weather predictions are combined with remote sensing (NOAA-AVHRR) based estimates of the global albedo, NDVI and surface temperature for the direct calculation of net radiation, sensible heat fluxes and evapotranspiration rates at the national level in Denmark (Boegh et al., 2002b). Three field stations, representing agricultural land (Foulum), a beech forest (the EUROFLUX setup in Sorø) and a conifer forest (Ulborg), provide the basis for assessing the validity of both the weather predictions and the computed atmospheric fluxes.

Weather predictions

The predicted weather conditions at 12 GMT are used as proxies for the air temperature and air humidity at the time of satellite passage (12.30 – 15.00 GMT). The root mean square error (rmse) of the assessed (proxy) air temperature is 1.9 °C which is lower than the rmse of 3- 5 °C which are reported for remote sensing based estimates of in-situ air temperature (ie Prince et al., 1998). Generally, the weather predictions tend to be lower than the field measurements. This may well be explained by the difference between prediction level (approximately at 30 m height) and measurement level (a few meters above the canopy).

For the air humidity, the rmse is 204 Pa. This is comparative to the accuracy with which air humidity can be assessed using microwave remote sensing observations above the ocean (Schüssel et al., 1995). Remote sensing based estimation of air humidity in heterogeneous landscapes is not yet feasible (Czajkowski et al., 2002). Except for the Ulborg site in Western Jutland, the HIRLAM predicted (proxy) air humidity tend to be underestimated.

Evapotranspiration rates

Net radiation is calculated on the basis of the satellite observations of global albedo and brightness temperature and the climate predictions which are used to assess the incoming longwave radiation. The soil heat flux is strongly related to the net radiation at the soil surface, and it can therefore be assessed using the NDVI which is related to the radiation extinction by the canopy. The sensible and latent heat fluxes are calculated using the method described in Boegh et al. (2002a) whereby an empirical equation for the vapour pressure at the surface is introduced to facilitate mathematical solutions for the atmospheric resistance, the surface resistance and the evapotranspiration rates.

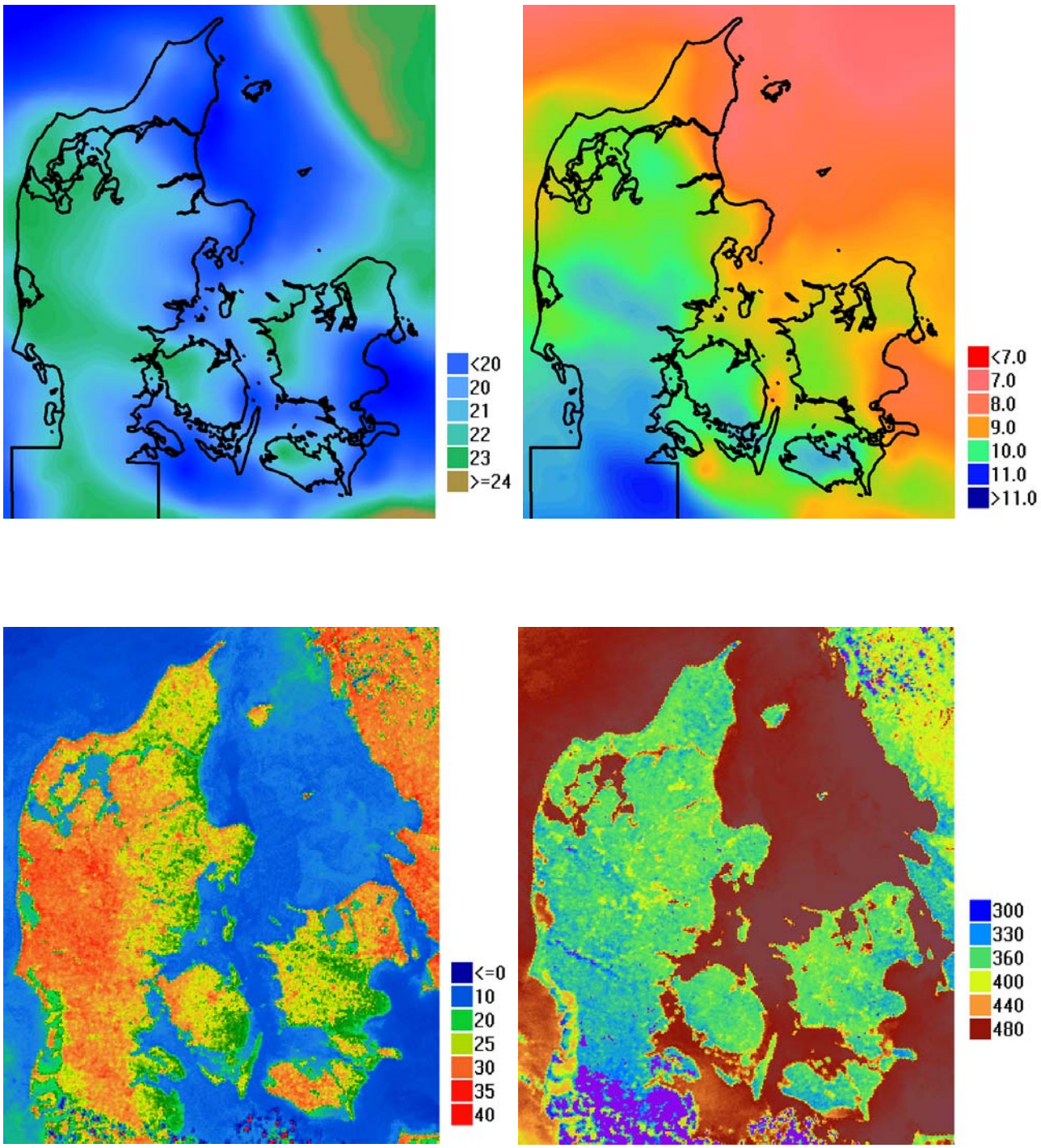

Figure 5-1. HIRLAM predicted air temperature in degrees Celsius (upper left) and air humidity in g/m3 (upper right); 29th April 2000 at 12.00 GMT. Surface temperature in degrees Celsius (lower left) and net radiation in W m^{-2} (lower right) calculated from NOAA-AVHRR; 29th April 2000 at 14.00 GMT. The dark blue dots in the lower part of the surface temperature image (lower left) illustrates very low temperatures due to cloud coverage. The observed cloud coverage region occurs in concurrency with the area where HIRLAM predicts high air humidity (upper right).

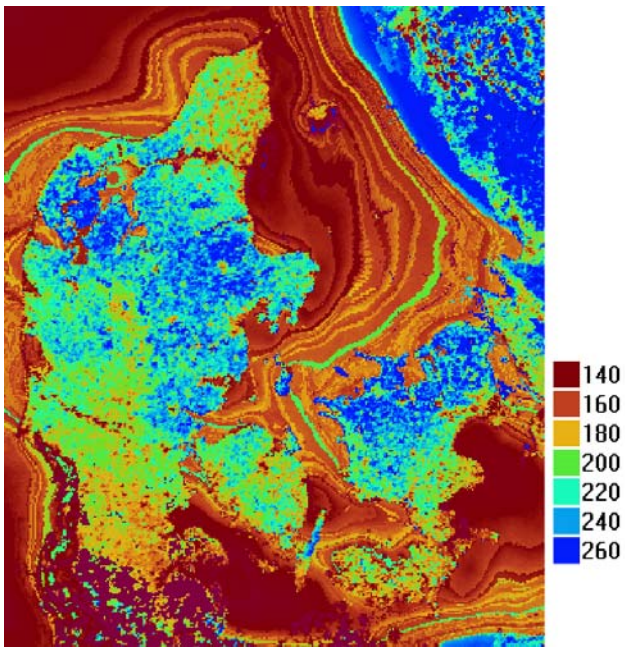

Figure 5-2. Evapotranspiration rates in W m^{-2} calculated using HIRLAM weather predictions and NOAA-AVHRR observations; 29th April 2000 at 14.00 GMT.

An example on the HIRLAM and satellite inputs is shown in Figure 5-1 together with the calculated evapotranspiration rates in Figure 5-2. Due to the encirclement by sea shorelines, there is a significant spatial variation in air temperature and air humidity in Denmark. In particular, the effect of the sea breeze circulation system is responsible for the intrusion of cooler air temperatures along shorelines which increases the sensible heat flux and suppresses the evapotranspiration rates (Boegh et al., 2002b). In the presented results (Figure 5-1 and Figure 5-2), the effect of cooler air temperature on the evapotranspiration rate is observable in the Northern and Eastern parts of Denmark. Because of the high surface temperatures of the drier sandy outwashed plain in Western Jutland, the evapotranspiration rates are also lower in this part of the country. The major cities in Denmark also have high surface temperatures and low evapotranspiration rates (ie. Copenhagen). The spatial pattern of the calculated evapotranspiration rates at sea are governed mainly by the HIRLAM predicted air temperature.

The comparison between calculated and measured atmospheric heat fluxes in Foulum (agriculture), Sorø (beech forest) and Ulborg (conifer) disclose a linear relationship with a rather large degree of scattering. The root mean square errors are found to be 67 W m^{-2} and 80 W m^{-2} for the latent and sensible heat fluxes, respectively (Boegh et al., 2002b). It is concluded that improved accuracies of both the weather (proxied) predictions and the processed satellite image quality are warranted to advance the presented approach for calculating evapotranspiration rates in Denmark. In order to improve satellite data quality, spatially distributed information on atmospheric conditions should be allowed as inputs for the atmospheric correction of satellite (instead of single values representing all Denmark).

5.2 Summary

The importance of using spatially distributed weather conditions for remote sensing based calculation of evapotranspiration rates at larger scale are testified, and the benefits of using meteorological predictions by a regional weather forecast model for 1) atmospheric correction of satellite imagery and 2) calculation of evapotranspiration rates are highligthed.

The weather predictions at 12 GMT are shown to be reasonable proxies for the atmospheric conditions at the time of satellite passage, and the feasibility of using HIRLAM predictions for the atmospheric correction of satellite imagery is encouraging. Therefore, the combination of the weather predictions and timeseries of atmospheric corrected satellite observations are useful for the calculation of evapotranspiration rates in Denmark. In Denmark, the sea breeze effect and the distinct (observed) surface properties of the sandy outwash plain in Western Jutland has significant impact on the spatial distribution of evapotranspiration rates in Denmark. The scatter between predicted and measured evapotranspiration rates is expected to reduce with increased accuracies in both the weather predictions and the satellite observations.

6 Aggregation

Microscale heterogenieties, ie surface changes in the spatial domain of the order of 100 m to 1000 m, are very important for the total grid averaged surface stress and the grid averaged surface heat fluxes. The need to find practical and fast aggregations routines for the roughness is a well-known problem (eg Viterbo 1996, Sellers et al. 1996). Area-averaging the roughness by simple area-weighted averaging is not physically sound. This is due to the highly non-linear turbulent responses of the atmospheric flow.

Recently an objective, physically-based model that takes the turbulent response of the atmospheric flow into account for every roughness step change in the terrain was developed. The solution is numerical fast because the linearized flow equations are solved by Fast Fourier Transforms (Hasager and Jensen, 1999). The model is a so-called microscale aggregation model.

Briefly described the microscale aggregation model needs input of high-resolution maps of roughness and surface temperature and a known wind and air temperature at the computational level (eg the lowest level of HIRLAM approx. 36 m). The flow equations include correction for atmospheric stability. This is iteratively calculated in every pixel. The surface shear stress and friction velocity is calculated pixelwise in the domain and area-averaged non-linearly to the desired grid cell size of a mesoscale climate model. The output is an effective roughness length for momentum. This will always be larger than a logarithmic average due to the *added* effect of non-equilibrium flow conditions. The effective scalar roughness length (for heat, water vapour and passive scalars) generally will be smaller than for equilibrium conditions. This is well known (Wood and Mason, 1991). The scalar roughness lenght is estimated from the high-resolution maps land cover maps, surface temperature maps and maps of leaf area index.

The roughness for momentum is not only dependent upon the roughness of field patches but is also dependent upon the amount of hedges in the landscape. The roughness for momentum from field patches is treated in section 6.1, the roughness for momentum from hedges is treated in section 6.2 and the scalar roughness is treated in section 6.3.

6.1 Roughness for momentum

The aerodynamic roughness for momentum, z_0, in m is the height above the surface where the wind speed is zero. The local roughness in each patch is calculated from meteorological observations of wind speed and the temperature gradient. For a full description please refer to (Stull, 1991).

Area-averaging the local roughnesses by simple area-weighted averaging is not physically sound. This is due to the highly non-linear turbulent responses of the atmospheric flow. It occurs when the flow is advected from one patch to the next with variations in roughness, temperature and humidity between them. Different turbulent responses are found from smooth to rough, cool to warm, dry to humid, and the reverse, and for any combination of these cases. The various changes are all described by internal boundary layer theory (eg Kaimal and Finnigan, 1994) and a practical solution is found (Hasager and Jensen, 1999).

Satellite remote sensing data of the land surface characteristics is the key information for the microscale aggregation model. From high-resolution optical satellite scenes it is possible to map the land cover types in various regions. This information is then used for assigning relevant aerodynamic roughness lenghts in the region of interest. The roughness lengths in each local type of land cover is usually known from micrometeorological experiments, either in a given project or from values cited in the literature. The aerodynamic roughness assigned to a local patch should be measured such that upwind roughnesses are not influencing the signal. For forests this distance is shown to be dependent of atmospheric stability and the roughness of the forest (Dellwik and Jensen 2000).

The microscale model – in it´s simplest form – only valid for neutral static stabilility for the calculation of the momentum flux, is sketched in Figure 6-1.

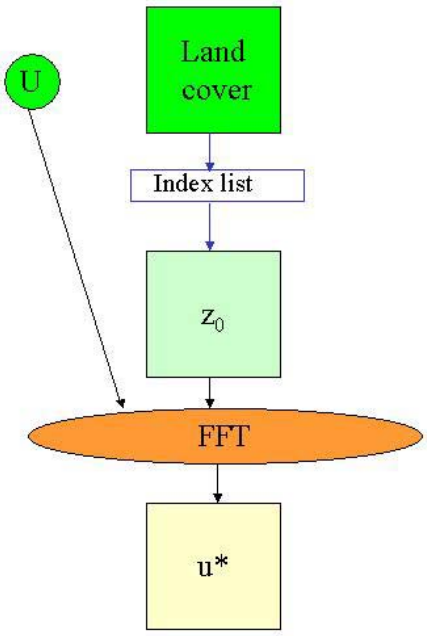

Figure 6-1. Microscale aggregation model for momentum flux in neutral static stability. The squares are two-dimensional maps in the horizontal domain of land cover, local roughnesses (z_0) and friction velocity (u_*) per pixel. The index list assigns roughness values to the land cover map. The wind speed (U) is at the compuational level. The model calculations are done with Fast Fourier Transform (FFT).

The model inputs are a land cover map retrieved from satellite classification analysis, an index list linking a local roughness to each land cover type (eg per month) and a wind speed at the computational level. The output is a map of the friction velocity (u_*) in m s^{-1}. From this the effective friction velocity $<u_*>$ is calculated from

$$< u_* >= \sqrt{\frac{1}{n_1 n_2} \sum_{x=1}^{n_1} \sum_{y=1}^{n_2} u_*^2(x,y)} \qquad (6.1)$$

and the effective roughness $<z_0>$ is calculated from

$$< z_0 >= z\left[\exp(\frac{\kappa u}{< u_* >}) \right]^{-1} . \qquad (6.2)$$

In this simple form the microscale model is applied for Denmark based on the CORINE land cover map (EEA, 1992) with a 250 m * 250 m resolution and the Areal Information System (AIS) map (Danish Areal Information System, 2001) with a 25 m * 25 m resolution. This work is documented in (Hasager et al., 2002). The roughness value per land cover type for the AIS map is listed in Table 6-1. The local values of roughness are area-averaged up to the grid cell size of the DMI-HIRLAM-D05 model. This has a grid resolution of 15 km * 15 km.

Table 6-1. Roughness value z_0 in m per land cover type for summer and winter in the index list for the AIS map. The percentage land cover is shown.

	Summer	Winter	Land area (%)
Unknown	0.01	0.01	0.39
Water	0.002	0.002	0.00
Sand	0.03	0.03	0.08
Marsh	0.08	0.08	2.03
Grass heath	0.08	0.08	1.08
Permanent short grass	0.03	0.03	0.22
Grazing	0.08	0.08	4.21
Meadow	0.08	0.08	0.31
Bush/grass heath	1	1	0.22
Bush/heather	1	1	0.28
Bush/forest	1.8	1.8	0.68
Deciduous forest	1.8	1.8	1.09
Coniferous forest	1.8	1.8	0.56
Meadow	0.08	0.08	0.32
Agriculture	0.05	0.01	38.45
Discontinuous urban	0.5	0.5	3.58
Continuous urban	1.2	1.2	0.56
Beech forest	1.8	1.8	2.00
Young forest	1.8	1.8	0.12
Spruce plantation	1.8	1.8	5.46
Mixed forest	1.8	1.8	18.32
Mountain pine	1.8	1.8	0.26
Oak forest	1.8	1.8	0.00
Lark forest	1.8	1.8	0.02
Clearing	0.3	0.3	0.02
Sparse coniferous	1.8	1.8	0.27
Heather	0.08	0.08	0.12
Peat bog	0.08	0.08	0.15
Set-aside	0.08	0.08	0.04
Juniper heath	0.08	0.08	0.02
Heathland	0.08	0.08	0.24
Agriculture/grassland	0.05	0.01	19.33

The land cover classification maps from Foulum based on Landsat TM and SPOT (see scetion 4.3) from 1998 and 1999 are used to assess the effect of including a large number of agricultural classes in the microscale aggregation model. It is concluded that these classified Landsat/SPOT scenes are the most accurate inputs. However also the AIS land cover map has a sufficient resolution and accuracy, except for the land cover type defined as non-vegetated, please refer to Hasager et al. (2002c). The CORINE land cover map on the other hand, is too coarse for the typical landscapes in Denmark. This is explained by the fact that many patches in Denmark are in the order of 250 m or less, and as the CORINE map has a resolution of 250 m this is not sufficient. The AIS map has a resolution of 25 m.

The work includes a comparison of the $<z_0>$ model results to field observations in Børglum, Foulum and Tystofte on a monthly basis. It is found that the effective roughness is very well modelled at Børglum. However in landscapes with hedges the modelled value of $<z_0>$ is too small (Foulum and Tystofte). Therefore a theoretical study on the effect of hedges is carried out as well as a quantification of the hedges in Denmark (in section 6.2).

Directional effects

The aggregated roughness in a grid cell may be dependent upon the direction of the wind. This is e.g. shown in Hasager and Jensen (1999) where the directional effect as seen by a meteorological mast is compared to model results.

The Corselizte area at eastern Falster is chosen for a demonstration case in the present project. The roughness map of the Corselitze area is based on the AIS map in summer conditions and the friction velocity is calculated for neutral stability and a wind speed of 5 m s^{-1} at 36 m from four directions (N, E, S and W). Figure 6-2 shows the resulting map of u_* for westerly wind. The horizontal resolution is 25 m by 25 m for the 12 km by 12 km area. It is clear that the friction velocity is large over land and low over the sea. The variability in u_* along the horizontal transect is graphed in Figure 6-3. From this it is seen that u_* is large over the forest, medium over the agricultural area and low over the sea. Further it is clear that u_* is maximum at the leading forest edge. Over the sea u_* is minimum near the coast and very gradually increasing downwind. For easterly wind the maximum in u_* is again found at the leading edge of the forest and is decreasing downwind. The reason why the maximum in u_* is more pronounced for easterly wind than westerly, is due to the fact that the roughness of the sea is very low (lower than that of the agricultural area), hence the step change is larger and the non-linearity of the turbulent response is more pronounced.

The directional effect for the whole 12 km by 12 km grid cell at Corselitze is listed in Table 6-2. It is seen that $<z_o>$ and $<z_0>/z_{0a}$ are largest for easterly wind and smallest for northerly wind. The effect of wind direction may more significant at higher grid cell resolution.

The effect of wind direction at all the 15 km by 15 km grid cells used in the HIRLAM model (section 7-5) is tested for wind directions from west and south and the results are graphed in Figure 6-4. It is clear that the directional effect is larger in winter than is summer. For the present study the effective roughness maps based on westerly (the dominant) wind direction is used.

Table 6-2. Effective friction velocity and ratio between effective and log-averaged friction velocity for four wind directions, case study results for Corselitze based on AIS summer roughness.

	West	North	East	South
$<z_o>$ (m s^{-1})	0.0217	0.0159	0.0227	0.0160
$<z_0>/z_{0a}$	5.89	4.30	6.16	4.35

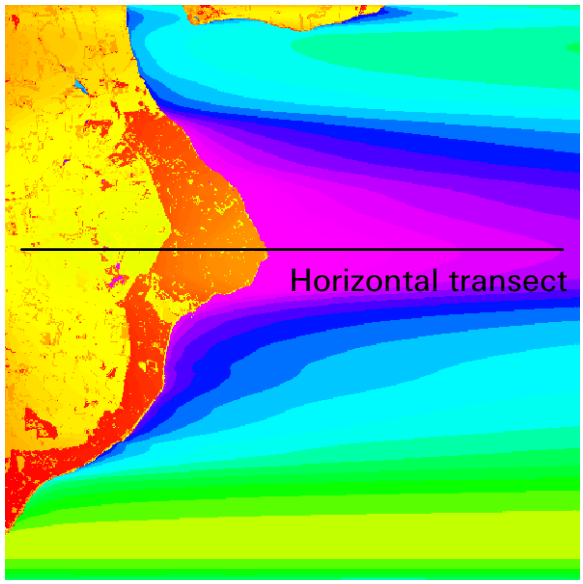

Figure 6-2. Corselitze case study on variations in friction velocity based on the AIS map. The wind is from west at 5 m s^{-1} at 36 m and neutral static stability. The colour scale enhances spatial variations where the minimum is light purple (0.16 m s^{-1}) and the maximum is dark red (0.73 m s^{-1}). The domain is 12 km by 12 km. The position of the horizontal transect in Figure 6-3 is shown.

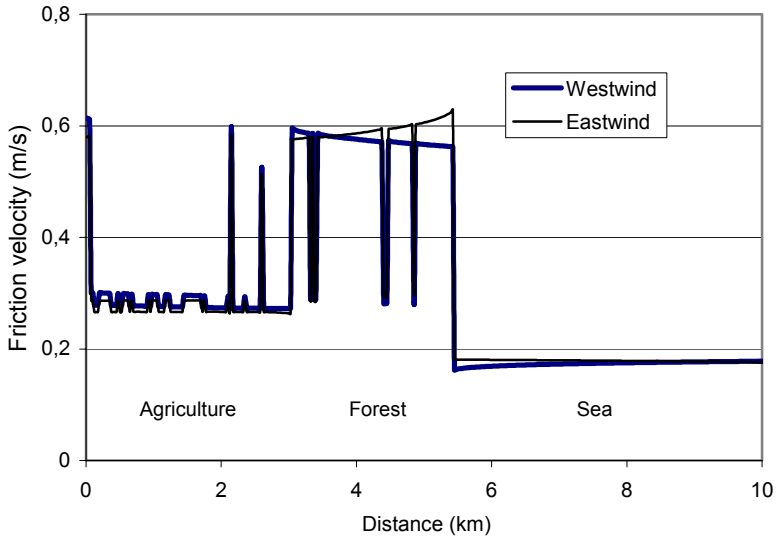

Figure 6-3. Friction velocity in horizontal transect in the Corselitze case study for westerly and easterly winds. The location of the profile is given in Figure 6-2.

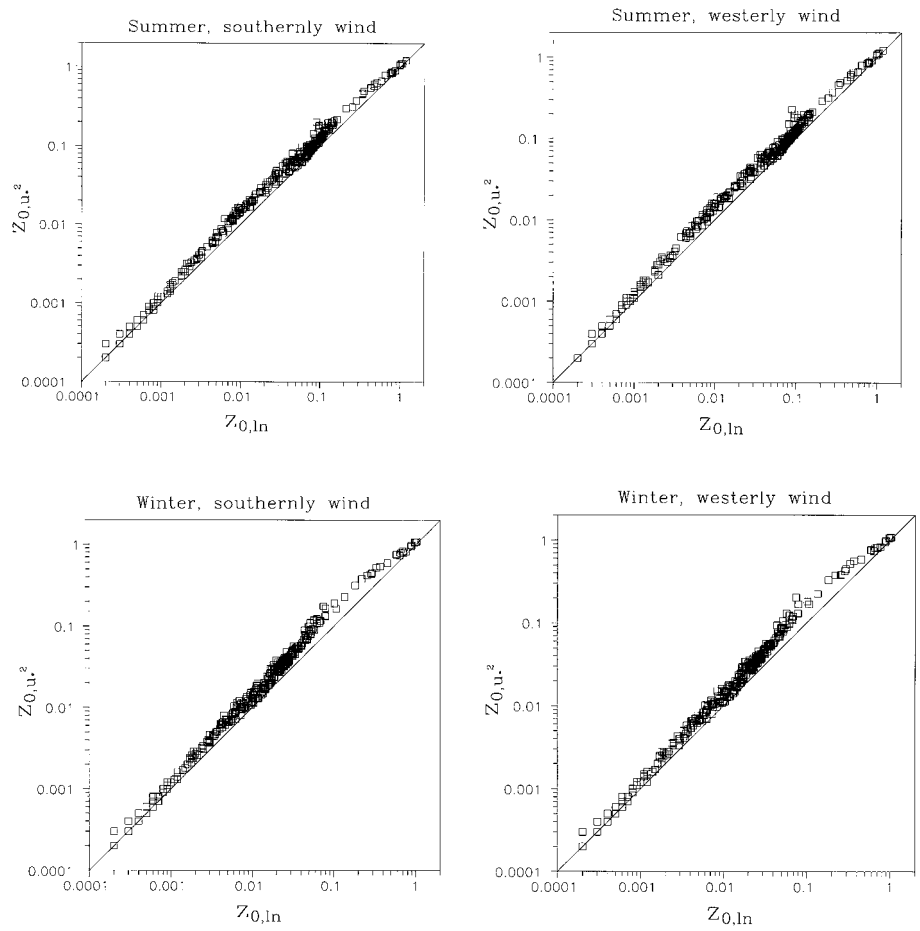

Figure 6-4. The log-average roughness on the x-axis and the effective roughness for all grid cells of 15 km by 15 km relevant for the HIRLAM model over Denmark. The roughness values are based on the AIS map is summer and winter and the results are for westerly and southwesterly winds.

6.2 Hedge row roughness

Theoretical aspects

The effective roughness $<z_0>$ of landscape inhomogenieties due to field patch variations is considered in section 6.1. In addition to the non-linear patch effect, the effect of singular obstacles is considered in the following. Hedge rows are notable in the Danish landscape and hence given special attention.

From a theoretical study described in (Hasager et al., 2002) an approximate formula for the additional roughness from hedge rows is derived

$$\frac{z'_0}{<z_0>} = \frac{1}{2}\frac{h}{D}\frac{c_D}{\kappa^2}\left(\ln\frac{h}{<z_0>}\right)^3 . \qquad (6.3)$$

The quantity z_0' is the amount that has to be added to $<z_0>$ in order to get the total roughness. The height of the hedges is h and the distance between them is D. c_D is the drag coefficient of the hedges and 6 is the von Karman constant.

In a numerical example with h = 4 m, D = 200 m, c_D =0.5 and z_0 = 0.2 m the formulation gives $z_0' = 0.8 \langle z_0 \rangle$.

Statistics on hedges in Denmark

The digital map Top10DK (National Cadastre and Survey, 1995-2000) is analysed with respect to hedges in Denmark (excluding Bornholm). Table 6-3 lists the mean distance between hedges in six Danish regions. The analysis is based on grid cells of 15 km * 15 km. The maximum mean distance of 1018 m between hedges is found in a grid cell located on eastern Lolland and the minimum mean distance of 216 m is found in a grid cell in western Jutland. Hence the density of hedges is approximately five times larger in western Jutland than on eastern Lolland.

The mean hedge distances are calculated from an assumption that the hedges are spaced parallel to each other within the grid cell. This is approximately true in western Jutland where the hedges are situated crosswind to the dominant wind direction in order to provide lee effects. In the eastern parts of Denmark hedges are often situated "randomly" and reflects the outlay of each farmers fields (land registrer). This means that the number of hedges is even smaller than calculated in Table 6-3 in the easterly regions (Lolland-Falster, Sjælland) for the dominant wind direction.

The total area covered by hedges is very small. Assuming a width of hedges of 10 m, the minimum area covered is 1.0 % (eastern Lolland) and the maximum area covered is 4.6% (western Jutland). But due to non-linear effects described above, the influence of hedges to the total kinematic stress is much larger than weighted by the covered area.

Table 6-3 Mean distance between hedges in six Danish regions

	Mean distance (m)
Lolland-Falster	900
Sjælland	781
Østjylland	650
Nordjylland	434
Fyn	412
Vestjylland	296

The meteorology mast at Foulum is situated in a grid cell typical for Vestjylland, the mast at Tystofte is placed in grid cell typical for Sjælland but the mast at Børglum is placed in a grid cell atypical for northern Jutland. In the vicinity (footprint) of the Børglum mast, the local area is practically devoid of hedges in a 4 km * 4 km area. This makes the location of the mast special indeed. As stated previously, the microscale $\langle z_0 \rangle$ model result compares very well to mast observations at Børglum but is negatively biased for the Foulum and Tystofte cases.

Microscale model results on hedge roughness

The added roughness effect is estimated as a function of hedge density from synthetic data used in the microscale aggregation model. It is not feasible to run the microscale model on the national level eg at 5 m resolution. The added roughness is defined as the effective roughness including hedges minus the average effective roughness is a patchy landscape without hedges.

The synthetic data consists of a checkerboard terrain with hedges spaced at different distances. The synthetic data simulate typical summer and winter conditions for Tystofte and Foulum. It is found that the added roughness in summer is ~0.029 m for Tystofte and ~0.040 m for Foulum. In winter the added roughness is ~0.016 m. The results are found for an assumed hedge roughness of 2 m. The assumed roughness of the hedges is of some importance, however not well known (or well-defined). It is important to include the additional effect of hedges to the effective roughness. A simple equation is developed to quantify the extra roughness relevant in four regions (Hasager et al., 2002).

6.3 Scalar roughness

The overall goal of calculating the effective roughness for scalar transport is to achieve very precise area-averages of the scalar fluxes. For very large patches equilibrium conditions will apply, but for shorter horizontal length scales typical for instance in Denmark, non-equilibrium conditions will dominate the scalar surface fluxes.

Theoretical part

In surface-layer profile relations it has been customary to take the roughness length for temperature z_{ot} equal to z_o for momentum. However, especially if z_o includes the effect of separated flow over orography this can lead to quite erroneous results for the heat flux. In the following we will assume that z_o is the micrometeorological roughness, but as we will show below, z_{ot} is in general less than z_o. How much smaller depends on the type of the surface, and unfortunately also on the value of the friction velocity u_*. Recently the formal dependence was presented by Jensen et al. (2002) and is described in detail in the following.

Per definition we have

$$u_* r_a = \frac{\bar{u}}{u_*} = \frac{1}{\kappa}\left(\ln\frac{z}{z_o} - \Psi_M\left(\frac{z}{L}\right)\right) \tag{6.4}$$

where u_* is the friction velocity, r_a is the aerodynamic resistance, $\bar{u}$ is the mean wind speed, κ the von Kármán constant (≈ 0,4), z is the height above the displacement distance of the vegetation, and z_o is the aerodynamic roughness.

The correction function, Ψ_M which depends on atmospheric stability expressed by the Monin-Obukhov length

$$L = \frac{u_*^2}{\kappa \frac{g}{T}\theta_*} \tag{6.5}$$

is an empirically determined function (fitted analytical function). While r_a is the only limiting resistance for "deposition" of momentum, scalars[2] such as temperature and humidity have an additional resistance r_b because they are also limited by molecular diffusion through the viscous sub-layers that blanket all surfaces. Thus for temperature

$$u_*\left(r_a + r_b\right) = \frac{\theta - \theta_0}{\theta_*} = \frac{1}{\kappa}\left(\ln\frac{z}{z_{ot}} - \Psi_H\left(\frac{z}{L}\right)\right) \tag{6.6}$$

where θ is the temperature at height z, θ_0 is the surface temperature and θ_* is a scale for the temperature fluctuations ($\theta_* u_*$ is the sensible heat flux). z_{ot} is the roughness for temperature and Ψ_H is the Monin-Obukhov function for heat flux. Implicitly, eq.(6.6) assumes that the von Kármán constant as well as the displacement distance are the same for a scalar as for momentum. From eqs.(6.4) and (6.5) it follows that

$$u_* r_b = \frac{1}{\kappa}\left[\ln\frac{z_o}{z_{ot}} - \left(\Psi_H(\frac{z}{L}) - \Psi_M(\frac{z}{L})\right)\right] \tag{6.7}$$

This equation establishes the intimate connection between r_b and z_{ot}. In the following we shall neglect the subtle difference between Ψ_H and Ψ_M which then leads to the simple relationship

$$z_{ot} = \frac{z_o}{\exp(\kappa u_* r_b)}. \tag{6.8}$$

For smooth surfaces z_o and z_{ot} in eq.(6.7) are replaced by the molecular sublayer thicknesses ν/u_* and D/u_* respectively, leading to a fixed ratio between the momentum and temperature roughnesses and

$$z_{ot} = \frac{z_o}{\mathrm{Pr}} \tag{6.9}$$

where Pr is the Prandtl number (≈ 0.7) equal to the kinematic viscosity ν (≈ 1.5 10^{-5} m^2 s^{-1}) divided by the molecular heat conductivity D (≈ 2 10^{-5} m^2 s^{-1}). In practice this will occur only over water surfaces under low wind conditions (at about $u_* < 0.1$ m s^{-1} or $\overline{u}_{10}$ less than 3.3 m s^{-1}).

The above implies that $u_* r_b$ is constant for smooth surfaces. However, in general this product is not a constant but is in itself a function of u_*. Hence it is immediately seen from eq.(6.8) that z_{ot} is not a property of the surface alone but depends on the flow.

2 although temperature and humidity has some influence on buoyancy they are for some practical purposes regarded as passive contaminants

Expressions for r_b

As mentioned above $u_* r_b$ is not in general a constant. It is customary to describe its variation in relation to the roughness Reynolds number

$$\mathrm{Re} = \frac{z_0 u_*}{\nu} \tag{6.10}$$

The Figure 6-5, adapted from Garratt and Hicks (1973) shows such dependencies. The striking thing is the difference between rough surfaces consisting of bluff elements and rough surfaces consisting of plants (fibrous canopies). Note that there is an error in the label on the ordinate axis. It should have been $\kappa r_b u_*$.

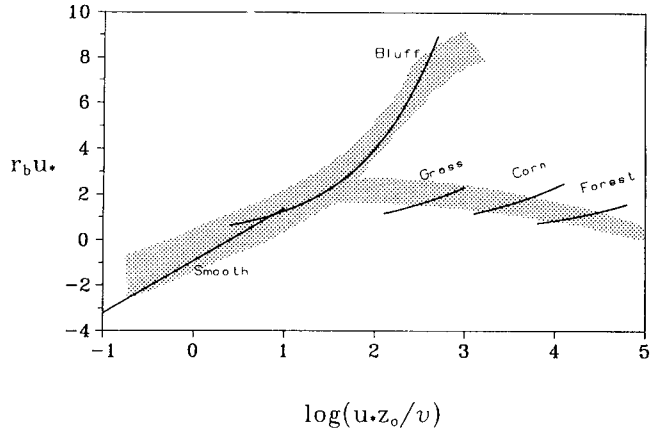

Figure 6-5. Adapted from Garratt and Hicks (1973). Note that there is an error in the label on the ordinate axis. It should have been $\kappa r_b u_*$.

The bluff body branch on the figure can be described by the relation

$$\kappa r_b u_* = c\,\mathrm{Pr}(\mathrm{Re})^{1/2}. \tag{6.11}$$

The types of land use categories where this equation applies ranges from water bodies that are aerodynamically rough ($u_* > 0.1$ m/s) over ice, snow and bare soils to cities. However, it turns out that for large z_0, the values of z_{0t} become unrealistically small (eg 10^{-40} m). So it is concluded that the relation in (6.11) is not realistic for large values of *Re*. Therefore a modified expression is sought.

It is suggested to express *Re* as a function of the length scale of typical materials over which the development of laminar layers at the urban surfaces takes place, e.g. bricks, roof materials etc. In fact the method is similar in concept to the one applied for plant canopies by Jensen and Hummelshøj (1995). In other words, the laminar layers do not scale with the height of the buildings but rather with the smaller scale features of the urban surfaces, e.g. roof tiles, windows, etc.

$$\mathrm{Re} = \frac{l u_*}{\nu} \quad l = \begin{cases} z_0 & \text{if} \quad z_0 < 0.05m \\ 0.05 & \text{if } z_0 \geq 0.05m \end{cases} \tag{6.12}$$

Thus by combining eqs. 6.8 and 6.12 we get

$$\ln \frac{z_0}{z_{0t}} = c \,\mathrm{Pr} \left(\frac{l u_*}{\nu} \right)^{1/2} . \tag{6.13}$$

The factor *c Pr* in the above equation is assesed to be about 0.4.

In the MKS unit system we thus have the following practical expressions

$$z_{0t} = \frac{z_0}{\exp(100\sqrt{z_0 u_*})} \qquad \text{for } z_0 < 0.05 \text{ m} \tag{6.14}$$

and

$$z_{0t} = \frac{z_0}{\exp(22\sqrt{u_*})} \qquad \text{for } z_0 \geq 0.05 \text{ m} \tag{6.15}$$

The values of z_{0t} are assessed for the non-vegetated land surfaces as described above.

Over water the description is complicated by the fact that the roughness z_0 depends on u_* through Charnock's formula (Charnock, 1955)

$$z_0 = \alpha \frac{{u_*}^2}{g} \tag{6.16}$$

where g is the constant of gravity and $\alpha \approx 0.015$ but where the exact value actually depends on the wave age, the fetch length and probably also the water depth at least over shallow water.

The plant canopy branch (see Figure 6-5) on the other hand has literally no dependence on Re. It was shown by Jensen and Hummelshøj (1995) that this is because the length scale z_o is not relevant. For example z_o for a forest is very large but what controls r_b, or more precisely the thickness of the viscous sublayers is the dimensions l of the fibrous elements. For plant canopies Jensen and Hummelshøj (1997) gives

$$r_b u_* = c \frac{\mathrm{Pr}}{LAI^{2/3}} \left(\frac{l u_*}{\nu} \right)^{1/3} \tag{6.17}$$

where *LAI* is the leaf area index, the Prandtl number has already been defined and c here is a constant of about 5. The length scale l is around $3*10^{-3}$ m for grass, grains and conifer forest and around $3*10^{-2}$ m for deciduous forest in leaves.

The remote sensing based Normalized Difference Vegetation Index (*NDVI*) is exponentially related to *LAI*. For Landsat TM the relation is (Boegh et al. 2002a)

$$LAI = 0.0051 * \exp(7.947 * NDVI). \qquad (6.18)$$

Summary on the equations for z_{0t}

In the expressions below we assume that all quantities are in MKS units.

<u>*Vegetated land*</u> (include grass, grains, decidouos and conifer forest)

$$z_{ot} = \frac{z_o}{\exp(\frac{5.85}{LAI^{2/3}} u_*^{1/3})} \qquad (6.19)$$

<u>*Bare land*</u> (include bare soil, ice, snow and urban areas)

$$z_{0t} = \frac{z_0}{\exp(103.3\sqrt{z_0 u_*})} \qquad \text{for } z_0 < 0.05 \text{ m} \qquad (6.20)$$

$$z_{0t} = \frac{z_0}{\exp(23.1\sqrt{u_*})} \qquad \text{for } z_0 \geq 0.05 \text{ m} \qquad (6.21)$$

<u>*Water*</u> (include smooth and rough water surfaces)

For smooth water, ie for $u_* < 0.1$

$$z_{ot} = z_o \; ; \quad z_0 = 0.1 \; \nu / u_* \qquad (6.22)$$

$\nu \approx 1.5\ 10^{-5}\ \text{m}^2\ \text{s}^{-1}$.

For rough water, ie for $u_* > 0.1$

$$z_{ot} = \frac{z_o}{\exp(100\,(z_0\ u_*)^{1/2})} \; ; z_0 = 0.015 \frac{u_*^2}{g} \qquad (6.23)$$

$g = 9.81\ \text{m s}^{-2}$.

Microscale aggregation model

There are two versions of the microscale aggregation model for the calculation of the momentum flux in non-neutral static stability and the sensible heat flux.

The first version (*"H"*) calculates u_*, ϑ, H and $\langle z_0 \rangle$.
The second version (*"z_{0t}"*) calculates u_*, ϑ, H, $\langle z_0 \rangle$ and z_{0t}.

Both versions can in principle – ie with the appropriate inputs – calculate also the water vapour flux and the deposition of passive scalars eg CO_2 directly. This part is briefly described in section 6.4.

<u>*Version "H"*</u>

The model is presented in (Hasager and Jensen, 1999) and applied in case studies in

- the Rhine Valley, Germany (Hasager and Jensen, 1999);
- Foulum, Denmark (Jensen and Hasager, 2000; Hasager et al., 2001);
- Sodankyla, Finland (Hasager et al. 2000;(Batchvarova et al., 2001))
- the Alpilles, France (Hasager et al., 2002a; Hasager et al., 2002b).

In this model version the roughness length for scalars (z_{0t}) is assumed to be a fraction of the roughness for momentum. This fraction can be changed as appropriate for the case, however the methodology is rather crude and improvements on this is implemented in the second model version.

A brief description of the first model version is given here. It is based on information on the surface temperatures retrieved from the thermal bands of optical satellites. The surface temperature from a satellite is not identical to the lower boundary temperature in the classical heat flux equations. The additional resistance between the two is the so-called kB^{-1} factor described by many (for references see Hasager 1997, page 18).

A diagramme of the model is shown in Figure 6-6. Two maps derived from satellite information, a land cover map and a surface temperature map, are used as input together with meteorological observations of wind speed, wind direction and air temperature at the computational level. The index list relates each land cover class to a local roughness value and the ratio *(r)* is the ratio between z_0/z_{0t} (eg in the range 0.1-0.0001). As an example a ratio of 0.01 seemed most appropriate in the Alpilles area in France when comparing the sensible heat flux to eddy correlation field observations and to radiosounding observations (Hasager et al., 2002a).

Stability effect

The stability has some influence on the effective roughness for a grid cell. The Corselitze area is used for a demonstration on the effect (as in section 6.1 on the directional effect). It is assumed that the surface temperature is homogeneous at 15 ºC for the area shown in Figure 6-2 and that the air temperature varies between 12 and 17 ºC at 36 m for a wind speed of 5 m s^{-1} from west. For unstable conditions $<z_0>$ is calculated larger than for neutral conditions. For stable conditions the effect is very small.

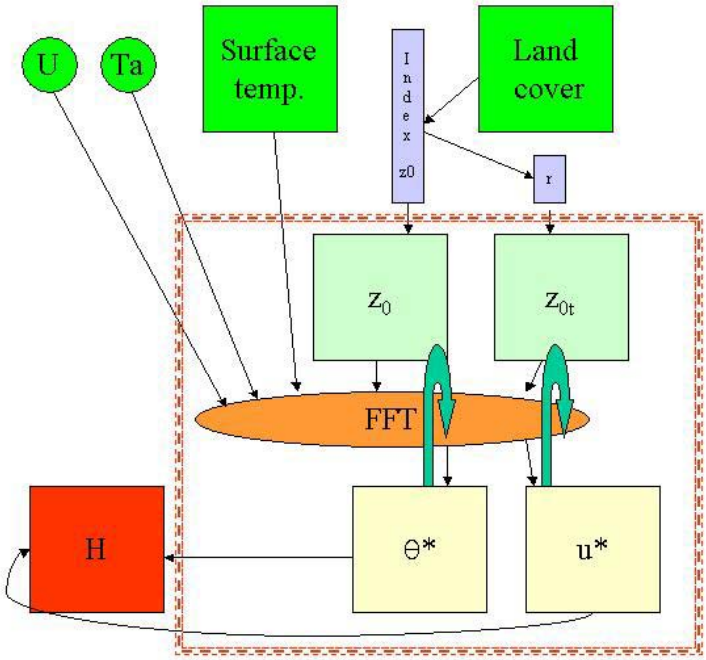

Figure 6-6. Schematic of the surface heat flux microscale aggregation model (Version "H") (Hasager and Jensen, 1999). The inputs are wind speed (U), air temperature (T_a) at the computational level and maps of surface temperature and land cover from satellite. The aerodynamic roughness map (z_0) and the scalar roughness length for sensible heat (z_{0t}) are assigned from the index-list. The model runs within the dotted red line. The atmospheric flow equations are linearized and solved by FFT. The output maps are the friction velocity (u_*) and the temperature scalar (2) both of which are found through iteration (indicated by the green curved arrows). The iteration is due to the stability function. The final output is a map of the sensible heat flux (H).*

Table 6-4. Results for Corselitze case study. Area-averages for a 12 km by 12 km area on the effective sensible heat flux <H>, maximum sensible heat flux H_{max} and effective roughness $<z_0>$ and the ratio $<z_0>/z_{0a}$ for variable air temperature aloft at 36 m and a constant surface temperature of 15 ºC.

T_a (ºC)	12	13	14	15	16	17
<H> (W)	54	34	16	0	-9	-11
H_{max} (W)	273	170	77	0	-56	-83
$<z_0>$ (m)	0.0252	0.0244	0.0233	0.0217	0.0209	0.0205
$<z_0>/z_{0a}$	6.85	6.62	6.33	5.89	5.67	5.56

Version "z_{0t}"

The new model development is an explicit calculation of the effective roughness for temperature $<z_{0t}>$. The approach is to apply a set of equations valid for local conditions for the different land cover types in the terrain for z_{0t} and iteratively solve these. It may be noted that for the vegetated land cover types an additional map of leaf area index (LAI) is included. The programme is sketched in Figure 6-4.

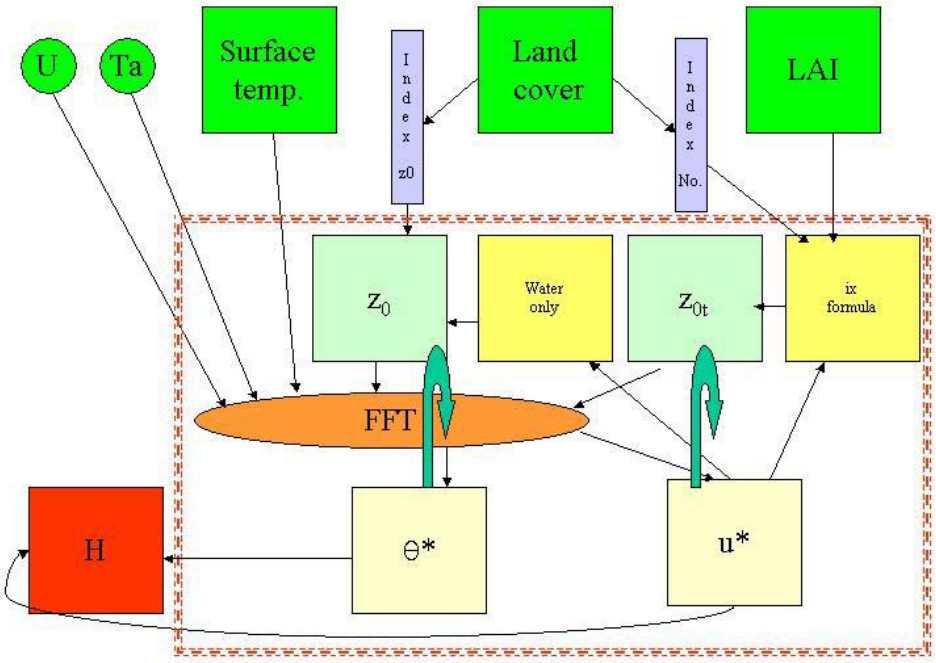

Figure 6-7. Schematic of the surface flux microscale aggregation model (Version "z_{0t}"). The inputs are wind speed (U), air temperature (T_a) at the computational level and maps of surface temperature, land cover classes and Leaf Area Index (LAI) from satellite. The aerodynamic roughness map (z_0) is generated from the index list except for water bodies where the Charnock's relationship is used. The index number and z_{0t}-equation (ix-formula) are prescribed for each land cover type to provide the z_{0t} map. The model runs within the dotted red line. The atmospheric flow equations are linearized and solved by FFT. The output maps are the friction velocity (u_*), the temperature scalar (2_*), the roughness map (z_0) and the scalar roughness map (z_{0t}) all of which are found through iteration (indicated by the green curved arrows). The iteration is due to the stability function and the Charnock's relationship. The final output is a map of the sensible heat flux (H).

The model runs on pc and the calculation for a 512*512 domain (eg a 15 km * 15 km grid cell with an input of 30 m * 30 m resolution) is achieved typically in less than 10 seconds computational time. Appendix II provides some additional details on the software.

Results from synthetic data

Synthetic data are used for the demonstration of the model behaviour in simplified cases.

Homogenous cases

Homogenous cases with only one type of land cover is presented first. Figure 6-8a shows for non-vegetated land ranging from ice thru snow and bare soil to urban area, the variation of z_{0t} as a function of z_0 (for u_* of 0.5 m s^{-1}) (eqs. 6.22-6.21). Figure 6-8b shows for forest, the variation of z_{0t} as a function of *LAI* (eq.6.19) and Figure 6-8c shows for water bodies, the variation of z_{0t} and z_0 as a function of u_* (eqs.6.25 and 6.26). It is seen that z_{0t} varies several orders of magnitude from around $1*10^{-1}$ to $1*10^{-9}$ m.

The ratio between z_0/z_{0t} is graphed for non-vegetated surfaces in Figure 6-9a, and for vegetated surfaces in Figure 6-9b. The ratio varies six orders of magnitude.

Heterogeneous cases

Heterogeneuos cases are presented next. For this purpose, checkerboard terrain is chosen with typical land use categories, variable surface temperatures and variable wind speed and air temperatures. Some results on the effective roughness, $<z_0>$, and the sensible heat flux, *H,* are already given in Hasager and Jensen (1999). In that work the effective roughness values are successfully compared to observations (Bradley.E.F., 1968) and to model results (Mason, 1988); (Schmid and Bünzli, 1995).

New findings obtained with the version "z_{0t}" programme are presented in the following. In Denmark in summer time typical land cover types have roughnesses and *LAI* as listed in Table 6-5a. The results from the microscale aggregation model on the effective roughness values for momentum and scalars are listed together with the logarithmic area-average of roughnesses (z_{0a}) that would be found for very large patches (of the order of 20 km patches). The landscape is assumed to consist of 256 m patches. The results are for a 5 m s^{-1} wind speed at the computational level at 8 m for neutral static stability.

It is noted that the roughness for momentum is a function of z_0 only and independent of *LAI*. For the cases on agriculture mixed with forest, the effective roughness ($<z_0>$) is around 3 times larger than the log-average roughness (z_{0a}). In sparse canopies with *LAI* equal to one, the effective scalar roughness ($<z_{0t}>$) is much smaller than the roughness for momentum. The kB^{-1} value is 6.5. A value of kB^{-1} of 2.3 is often assumed valid for porous vegetation (see Hasager, 1997, p18). For large *LAI,* the kB^{-1} approaches 2.3, however does not fully reach it. Mölder et al. (1998) list kB^{-1} from a number of experiments worldwide and the variation is very large.

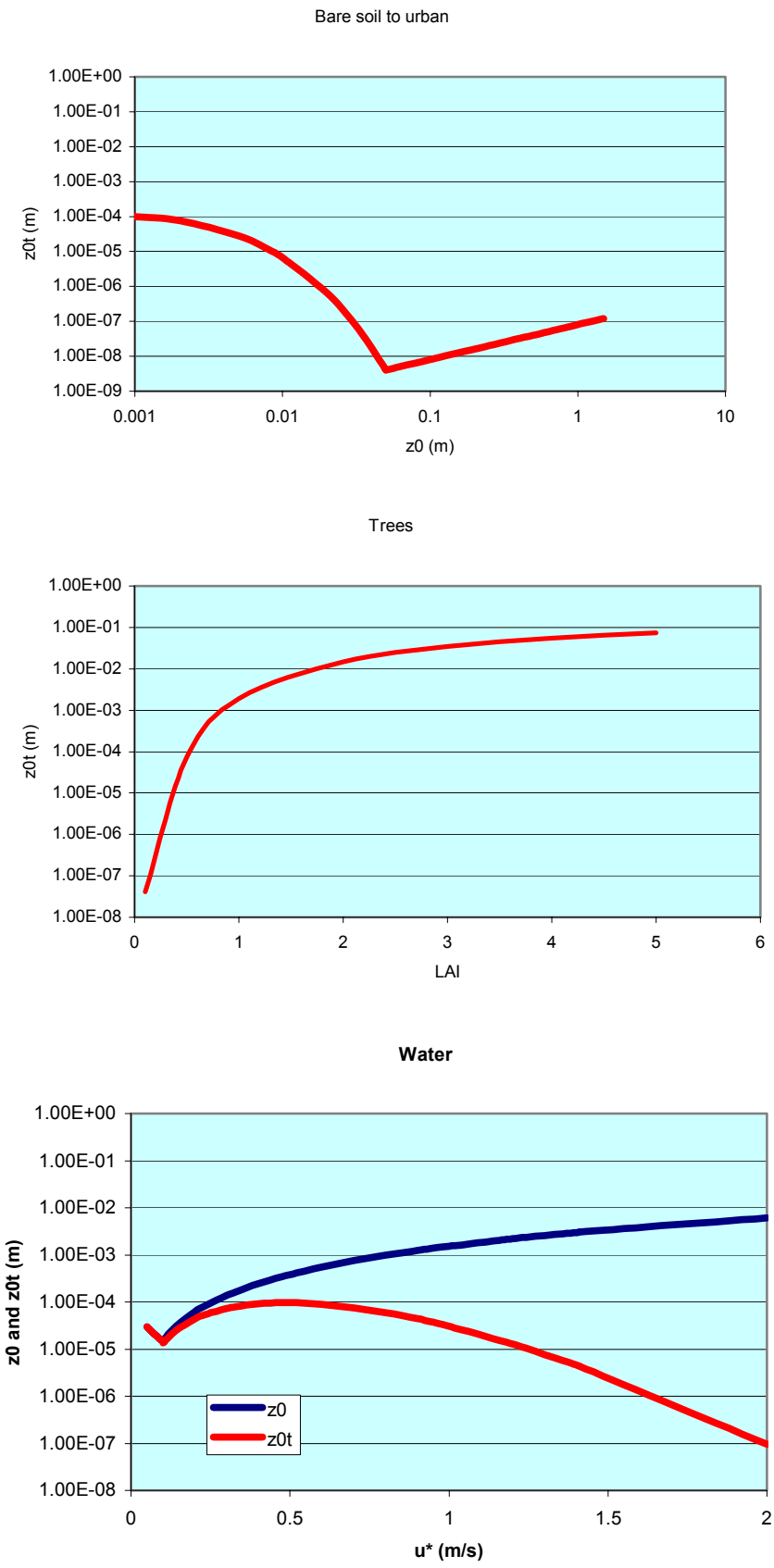

Figure 6-8. a) For non-vegetated surfaces z_{0t} as a function of $z_{0,}$ b) for forest z_{0t} as a function of LAI and c) for water bodies z_{0t} and z_0 as a function of u_*.

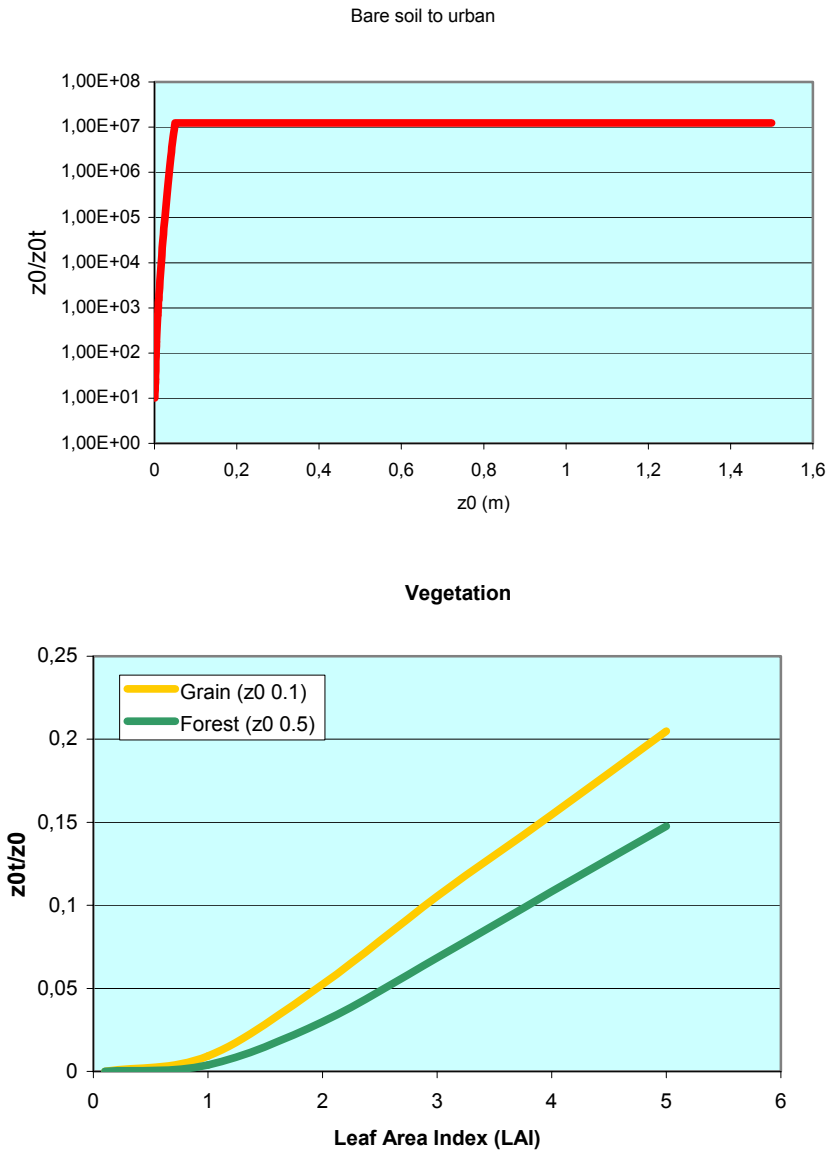

Figure 6-9. a) For non-vegetated surfaces the ratio z_0/z_{ot} as a function of z_0 and b) for vegetated surfaces z_0/z_{ot} as a function of LAI.

For cases on agriculture mixed with bush and on agriculture mixed with urban land cover, the effective roughness for momentum happens to be identical around 1.5 times larger than the log-average roughness. The effective roughness for scalar transport varies as a function of *LAI*. Only for cases of high *LAI* values is kB^{-1} close to 2.3. For low *LAI* values the kB^{-1} value is much larger (up to 5.2).

Results on land cover types mixed with water is also listed in Table 6-5 and it is noted that the effective roughness is very large compared to the log-average, especially when mixed with the very rough land cover types such as forest and city. In cases of agriculture mixed with water the kB^{-1} value is close to 2.3 for high *LAI* but larger (3.6) for low *LAI*. For forest mixed with water kB^{-1} is in all cases much larger than 2.3, reaching 7.0 for *LAI* equal to one. In cases of urban and city land cover mixed with water kB^{-1} is12 to 15.

Typical winter cases in Denmark are listed in Table 6-5b. It is assumed that the agricultural area is harvested and only bare soil prevails. The *LAI* of deciduous forest is very low, eg 0.5 and the resulting kB^{-1} is therefore very high (14) in such a landscape according to the microscale model results. For bare soil mixed with conifer forest of *LAI* equal to five, kB^{-1} is also 14. In landscapes of bare soil mixed with bushes with variable *LAI*, the kB^{-1} is 9.

Table 6-5a. Denmark synthetic summer cases of variable land cover type, roughness (z_0) and LAI and the microscale aggregation model results of effective roughnesses for momentum ($<z_0>$) and scalars ($<z_{0t}>$), the ratios between them and the logarithmic roughness for momentum (z_{0a}). $kB^{-1} = ln(<z_0>/<z_{0t}>)$.

Denmark summer			$<z_0>$(m)	z_{0a} (m)	$\frac{<z_0>}{z_{0a}}$	$<z_{0t}>$ (m)	kB^{-1}	$\frac{<z_{0t}>}{<z_0>}$
	agriculture	forest						
z_0 (m)	0.05	1.8						
LAI	1	1	0.93	0.30	3.1	1.4E-03	6.5	1.5E-03
LAI	2	2	0.93	0.30	3.1	1.0E-02	4.5	1.1E-02
LAI	3	3	0.93	0.30	3.1	2.3E-02	3.7	2.5E-02
LAI	5	5	0.93	0.30	3.1	4.8E-02	3.0	5.2E-02
	agriculture	bush						
z_0 (m)	0.05	0.5						
LAI	1	1	0.24	0.16	1.5	1.3E-03	5.2	5.5E-03
LAI	3	3	0.24	0.16	1.5	1.6E-02	2.7	6.6E-02
LAI	5	5	0.24	0.16	1.5	3.1E-02	2.1	1.3E-01
	agriculture	urban						
z_0 (m)	0.05	0.5						
LAI	1	0	0.24	0.16	1.5	4.7E-03	4.0	1.9E-02
LAI	3	0	0.24	0.16	1.5	1.4E-02	2.8	5.9E-02
LAI	5	0	0.24	0.16	1.5	1.9E-02	2.5	8.0E-02
	agriculture	water						
z_0 (m)	0.05	0.001						
LAI	1	0	0.01	0.01	2.1	4.0E-04	3.6	2.7E-02
LAI	2	0	0.01	0.01	2.1	8.8E-04	2.8	5.9E-02
LAI	3	0	0.01	0.01	2.1	1.2E-03	2.5	8.2E-02
LAI	5	0	0.01	0.01	2.1	1.6E-03	2.2	1.1E-01
	forest	water						
z_0 (m)	1.8	0.001						
LAI	1	0	0.90	0.04	21.5	8.3E-04	7.0	9.2E-04
LAI	3	0	0.90	0.04	21.5	4.3E-03	5.3	4.7E-03
LAI	5	0	0.90	0.04	21.5	6.7E-03	4.9	7.4E-03
	urban	water						
z_0 (m)	0.5	0.001						
LAI	0	0	0.17	0.02	7.7	6.6E-07	12.5	3.9E-06
	city	water						
z_0 (m)	1.2	0.001						
LAI	0	0	0.52	0.03	15.2	1.4E-07	15.1	2.7E-07

Table 6-5b. Denmark synthetic winter cases.

Denmark winter			$<z_0>$(m)	z_{0a} (m)	$\frac{<z_0>}{z_{0a}}$	$<z_{0t}>$ (m)	kB^{-1}	$\frac{<z_{0t}>}{<z_0>}$
	soil	deciduous						
z_0 (m)	0.01	1.8						
LAI	0	0.5	0.91	0.13	6.8	7.1E-07	14.1	7.8E-07
	soil	conifer						
z_0 (m)	0.01	1.8						
LAI	0	5	0.91	0.13	6.8	7.1E-07	14.1	7.8E-07
	soil	bush						
z_0 (m)	0.01	0.5						
LAI	0	1	0.02	0.01	2.8	2.0E-06	9.2	1.0E-04
LAI	0	3	0.02	0.01	2.8	2.0E-06	9.2	1.0E-04
LAI	0	5	0.02	0.01	2.8	2.0E-06	9.2	1.0E-04

Table 6-5c. Sodandyla synthetic winter cases.

Sodankyla winter			$<z_0>$(m)	z_{0a} (m)	$\frac{<z_0>}{z_{0a}}$	$<z_{0t}>$ (m)	kB^{-1}	$\frac{<z_{0t}>}{<z_0>}$
	snow	conifer						
z_0 (m)	0.01	1.4						
LAI	0	0.5	0.66	0.12	5.6	9.9-07	13.4	1.5E-06
LAI	0	1	0.66	0.12	5.6	9.9-07	13.4	1.5E-06

Table 6-5d. Alpilles synthetic summer cases.

Alpilles summer			$<z_0>$(m)	z_{0a} (m)	$\frac{<z_0>}{z_{0a}}$	$<z_{0t}>$ (m)	kB^{-1}	$\frac{<z_{0t}>}{<z_0>}$
	wheat	orchard						
z_0 (m)	0.05	0.39						
LAI	5	5	0.20	0.14	1.4	2.8E-02	1.9	1.4E-01
	wheat	sunflower						
z_0 (m)	0.05	0.18						
LAI	5	5	0.11	0.09	1.1	2.0E-02	1.7	1.9E-01
	orchard	sunflower						
z_0 (m)	0.39	0.18						
LAI	5	5	0.28	0.27	1.1	4.9E-02	1.7	1.8E-01

The microscale model has also been run for two typical other European sites. One is a winter landscape case in Sodankyla, ie a site in the north of Finland dominated by coniferous forest with low *LAI* interspersed with open snow covered landscape. The results are listed in Table 6-5c. The other is a summer landscape case in the Alpilles, ie a site in southern France consisting of a mixture of wheat, sunflower and orchard with high *LAI* (pers.comm. Albert Olioso, INRA, France). The results are listed in Table 6-5d. In Sodankyla the kB^{-1} value is high around 5 to 7 whereas in the Alpilles the kB^{-1} value is around 2.

The results are very approximate as the horizontal patch length scale varies greatly in different landscapes. In Denmark 256 m is a likely patch scale, however much smaller and larger fields, forests, water bodies and urban areas are also found in Denmark. In Sodankyla the typical length scale is much larger than 256 m (Batchverova et al., 2001).

An analysis on the importance of the horizontal patch length scale is undertaken for a case of agriculture mixed with forest both with a *LAI* of 5 typical in Denmark in the summer time. The results are listed in Table 6-6 and it is readily seen that the kB^{-1} value is approaching 2.3 for very large patches however does not reach the value even for patches of 8 km length scale. For shorter length scales the value of kB^{-1} is larger up to 3.0.

Table 6-6. Denmark synthetic summer cases of variable patch size of agriculture (z_0 0.05 m, LAI 5; forest z_0 1.8 m, LAI 5) and the microscale aggregation model results of effective roughnesses for momentum ($<z_0>$) and scalars ($<z_{0t}>$), the ratios between them and the logarithmic roughness for momentum (z_{0a}). $kB^{-1} = ln(<z_0>/<z_{0t}>)$

Horizontal scale (m)	$<z_0>$(m)	z_{0a} (m)	$\frac{<z_0>}{z_{0a}}$	$<z_{0t}>$ (m)	kB^{-1}	$\frac{<z_{0t}>}{<z_0>}$
64	0.99	0.30	3.3	4.8E-02	3.0	4.8E-02
128	0.97	0.30	3.2	4.8E-02	3.0	5.0E-02
256	0.93	0.30	3.1	4.8E-02	3.0	5.2E-02
512	0.89	0.30	3.0	4.9E-02	2.9	5.4E-02
1024	0.84	0.30	2.8	4.9E-02	2.8	5.9E-02
2048	0.77	0.30	2.6	4.9E-02	2.7	6.4E-02
4096	0.69	0.30	2.3	5.0E-02	2.6	7.2E-02
8192	0.62	0.30	2.1	5.0E-02	2.5	8.2E-02

Sensible heat flux

The effect of the $<z_0>/<z_{0t}>$ on the surface sensible heat flux is calculated on a simple synthetic summer case in Denmark. For very large patches equilibrium conditions will apply, but for shorter horizontal length scales non-equilibrium conditions will dominate. The results are reported in Table 6-7. It is again assumed that the patch size is 256 m, the wind speed is 5 m s^{-1} at the computational height at 8 m and that there is an overall neutral static stability. The potential air temperature at 8 m is assumed to be 15 ºC and the average surface temperature is assumed to be 15 ºC but with a local variation such that the local patches of agriculture and forest are varied ∀1 ºC. Further LAI is varied from 3 and 5. Without the new z_{0t} scheme the equilibrium sensible heat flux H_{eq} would be zero (see Hasager and Jensen, 1999). With the new scheme H_{eq} is not zero but this flux is not the true flux as it relies on the z_{0a} value instead of the $<z_0>$ value. The sensible heat flux (H) that pertains from the area including the non-linear effects is significantly different from zero. The results show that H is around ∀50 W m^{-2} for *LAI* of 3 and around ∀70 W m^{-2} for *LAI* of 5 (everything else being equal).

Table 6-7. Denmark synthetic summer cases of agriculture and forest with variable LAI and surface temperature.

	agriculture	forest	H (W m-2)	H_{eq} (W m-2)
z_0 (m)	0.05	1.8		
LAI	3	3		
T_0 (ºC)	16	14	-51.3	-11.5
T_0 (ºC)	14	16	55.6	13.1
LAI	5	5		
T_0 (ºC)	16	14	-65	-17.1
T_0 (ºC)	14	16	72	19.7

Results from satellite-based maps in Denmark

In Jutland, Denmark the area around Research Center Foulum is mapped from Earth Observation satellite. An example based on a Landsat TM scene is given here. The classified scene of land cover types (see section 4.3 for more detail) is shown in Figure 6-10 and the corresponding roughness lenghts are listed in Table 6-8. The leaf area index map is shown in Figure 6-11. The map is derived from NDVI and eq. 6.22. The microscale model has been run with these two maps as input together with an assumed wind speed of 5 m s^{-1} at 8 m height and neutral static stability. The area is approximately 10 km * 10 km.

Table 6-8. Land cover type and local roughness, Foulum, August 1999.

Land cover type	**z_0 (m)**
Spring barley/grass	0.05
Grazing	0.08
Spring barley	0.05
Maize	0.15
Beets	0.004
Winter wheat	0.05
Trees	1.8
Set aside	0.08
Peas	0.06
Oats	0.05
Winter barley	0.09
Water	0.001
Grass for cutting	0.03
Oil seed rape	0.07
Building	0.5

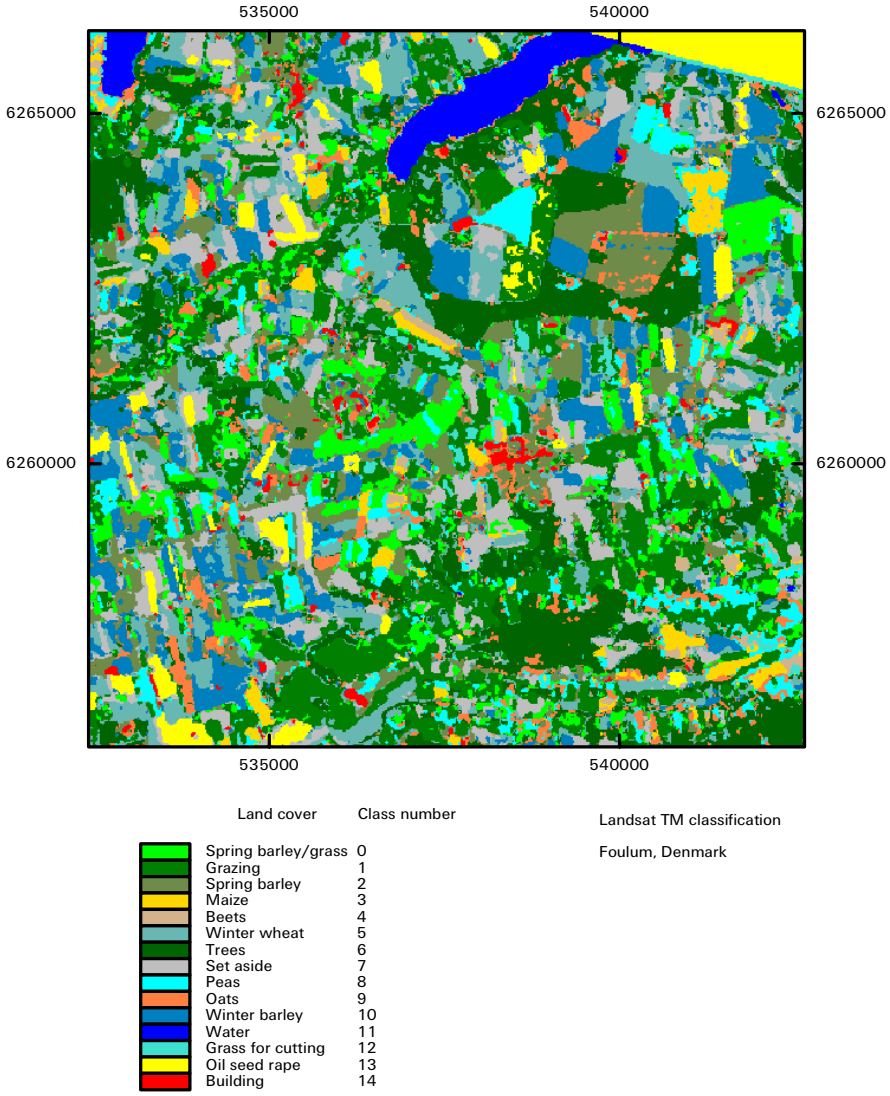

Figure 6-10. Land cover types mapped from Landsat TM in Foulum, Denmark in year 1999.

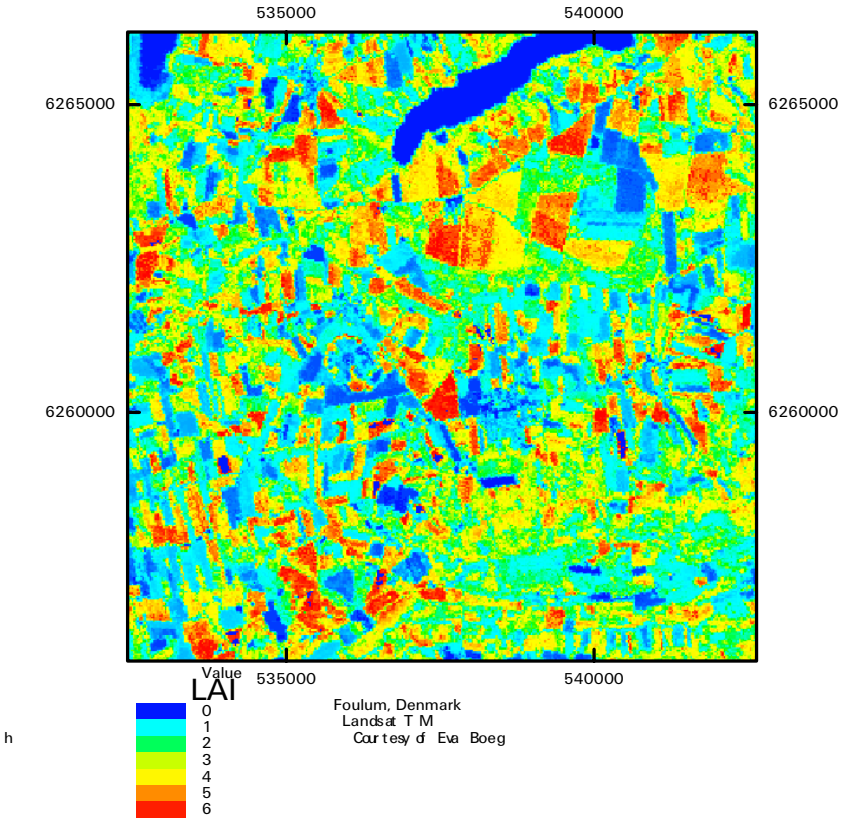

Figure 6-11. Leaf Area Index (LAI) map based on Landsat TM in Foulum, Denmark.

The microscale aggregation result for the Foulum area is that $<z_{0t}>$ is $1.8*10^{-3}$ m. Further is $<z_0>$ 0.31 m and z_{0a} 0.10 m, ie $<z_0>/ z_{0a}$ is 3.1. The kB^{-1} value is 5.2. The result compares well to the summer results from synthetic data for Denmark.

The mean *LAI* value in Foulum is 2.46 with a minimum of 0.005 and maximum of 7.5. The histogram distribution of *LAI* values is shown in Figure 6-12 and it is readily seen that the vegetation has very different values of *LAI*.

Variations in *LAI*, z_0 and the horizontal length scales give rise to non-linear effects on the area-averaged scalar roughness values. This is demonstrated with a few additional microscale model results. Assuming all land cover types to have identical *LAI* values. The model is run for *LAI* values ranging from 0.5 to 5.0. The result is shown in Figure 6-13. An interesting feature is that for the calculation of *LAI* equal to the mean value (2.4) the result is a larger $<z_{0t}>$ value ($7.91*10^{-3}$ m) than is found from the LAI map ($<z_{0t}>$ of $1.80*10^{-3}$ m). Ie the actual variations cause a smaller $<z_{0t}>$ than does a mean *LAI* of 2.4.

This finding underlines the importance of mapping *LAI* and z_0 at a detailed level prior to calculation of the effective scalar roughness.

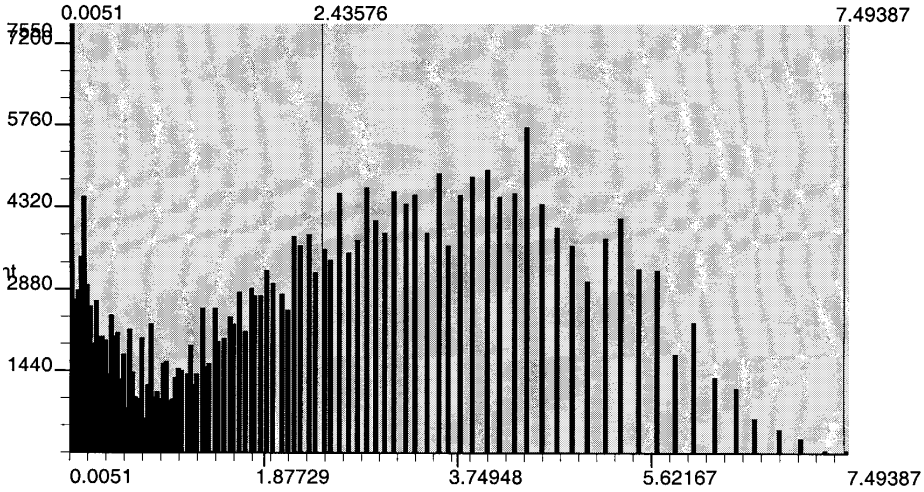

Figure 6-12. Histogram distribution of LAI values in Foulum based on Landsat TM. The x-axis is LAI, the y-axis is number of pixels. The mean value is indicated as well as the minimum and maximum values of LAI.

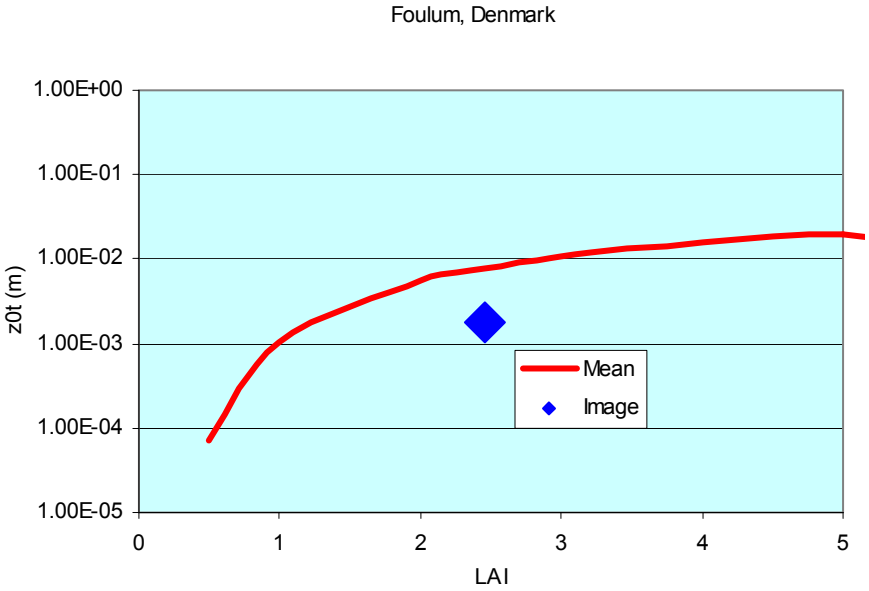

Figure 6-13. Area-average scalar roughness $<z_{0t}>$ for variable Leaf Area Index (LAI) as mean values over the area and from the LAI map (image).

6.4 Deposition modelling

The microscale model can be used in an inverse mode for the calculation of the upward and downward transport of passive scalars such as eg CO_2 and water vapour in a heterogeneous area. In this case the microscale aggregation model would need input of the concentration at the computational height (e.g. from a large scale model) and estimate a typical concentration at the lower boundary. The model would then calculate the surface flux to (or from) the region as a function of variations in aerodynamic roughness over the area, the leaf area in-

dex and the exact geographical location. The maps would be of the same resolution as the input (eg 30 m if based on Landsat TM).

6.5 Summary

A physically-based microscale aggregation model (Hasager and Jensen, 1999) is used for aggregating the roughness at 25 m resolution from the AIS land cover map assigned known local roughness lengths. The effective roughness is calculated into 15 km by 15 km grid cells for the HIRLAM weather prediction model per season for Denmark. The effective roughnesses are calculated for neutral stability and include the non-linear turbulent responses from stepwise changes in the roughness between all patches in the terrain. Comparison of the results to field observations in Foulum, Børglum and Tystofte reveals an underestimation of the effective roughness. This can be ascribed to the added roughness effect of hedgerows. From theoretical and modelling work on the added effect of hedges, an additional roughness is applied per grid cell as a function of the mean hedgerow density in Denmark quantified from the digital vector map Top10DK.

The microscale aggregation model is further developed within the project in respect to calculation of the effective roughness for scalar surface fluxes. The ratio between effective roughness lengths for momentum and scalars is often described by the kB^{-1} value around 2.3, ie a ratio of 0.1 between $<z_0>/<z_{0t}>$. It is shown that the kB^{-1} value and $<z_{0t}>$ vary as a function of the roughness for momentum, the leaf area index (*LAI*) and the patch scale. A simple study based on synthetic data that represents Danish summer conditions, shows that the new parametrization on $<z_{0t}>$ gives rise to a significant influence on the sensible heat flux. It is concluded, that a detailed mapping of the land cover classes, the local roughness values for momentum and the leaf area index is needed for an accurate calculation of the effective scalar roughness length.

7 Validation of HIRLAM weather forecasting

7.1 The HIRLAM system at DMI

The system is rather complex, consisting of preprocessing, analysis, initialization, forecast and postprocessing. The preprocessing involves conversion of observations to formats readable by the analysis and forecast model. Two statistically based analysis methods (optimum interpolation (OI) and 3 dimensional variational analysis (3Dvar)) have been developed in HIRLAM. Both have a very short range forecast (3 or 6 hours) as the first guess. OI was replaced operationally by the more sophisticated 3Dvar in two steps. In September 2000 3Dvar replaced OI on the largest model domain (G in Figure 7-1), and in December 2001 OI was replaced by 3Dvar on the smaller domain E in Figure 7-1 covering Europe and parts of the North Atlantic ocean. At present 4Dvar, an extension to 3Dvar including the time dimension, is in the test phase.

Two initialization methods, respectively a digital filter initialization and a non-linear normal mode initialization, have been developed for HIRLAM.

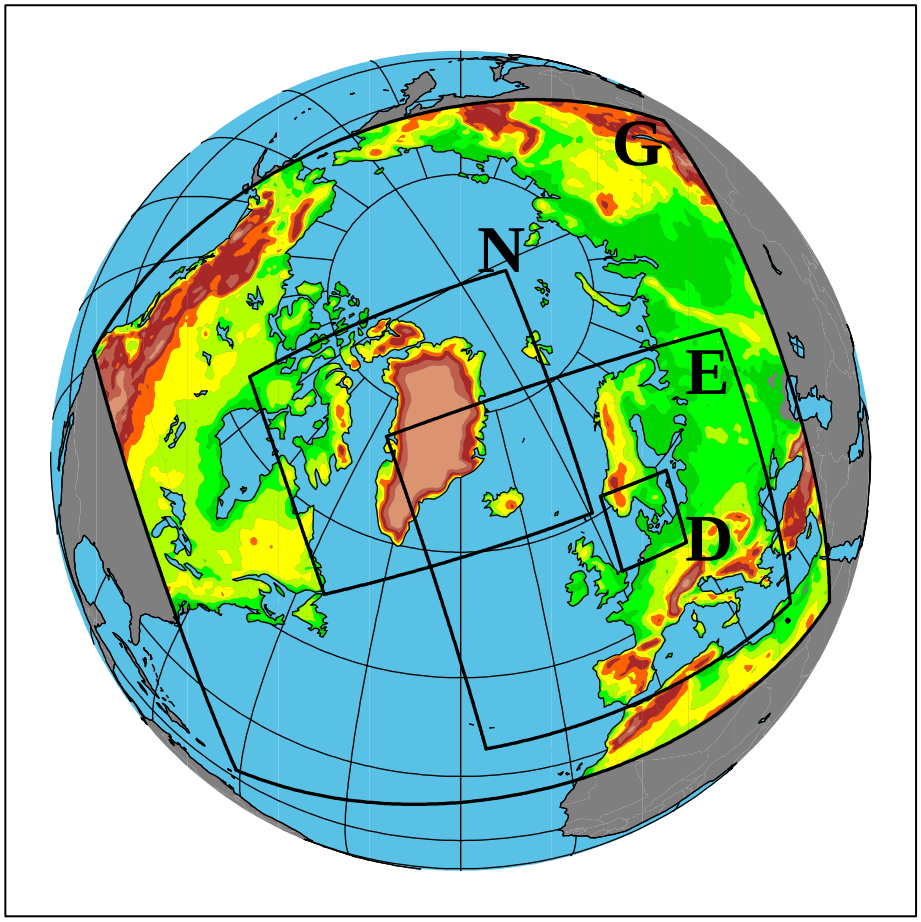

Figure 7-1. The operational DMI-HIRLAM integration areas.

The HIRLAM forecast model is a grid point model, but with a spectral version developed for use in the 4Dvar analysis. The forecast model integrates in time a discretized form of the governing equations of the atmosphere, which are the vector momentum equation, the thermodynamic energy equation, the equation of state, the mass continuity equation and budget equations for specific humidity and cloud water. The vertical momentum equation is approximated by hydrostatic balance. The discretization makes use of centred differences in space, horizontally on an Arakawa C grid. A vertical coordinate, which is terrain following near the surface and becomes pressure surfaces in the upper part of the atmosphere, is used. The time integration (time stepping) is done by the *leapfrog* method, which involves three time levels of the prognostic variables. In order to allow for reasonably long time steps in the integration the computations are split in an `explicit´ and a `semi-implicit´ part. The latter takes care of fast gravity waves such that the numerical stability criterion is governed by the meteorologically significant advection. To cope with the computational mode of the *leapfrog* scheme a time filter connecting even and odd time steps is applied.

The HIRLAM model can be run with either Eulerian advection or semi-Lagrangian advection. The latter allows for larger time steps than with Eulerian advection, but the penalty is some computational overhead connected with interpolations from departure points to the model grid.

Physical processes, taking place on space and time scales unresolved by the model, are parameterized. The processes are short wave (solar) radiation, long

wave (terrestrial) radiation, turbulence, convection, condensation and horizontal diffusion. The latter prevents piling up of energy on the smallest resolved scales. Energy budget equations, depending on the states of the surface, the soil below and the atmosphere above, are solved for the surface prognostic variables over land and ice surfaces. The state of the ocean, including the sea surface temperature (SST), is kept constant during a forecast. A wave model (WAM), interacting with the atmosphere model, has been developed in HIRLAM for future operational implementation.

A more advanced land surface scheme (the ISBA scheme (Rodrigues et al., 2002)) operating with a number of surface types, have been developed and is now ready for operational implementation. A surface analysis and soil assimilation package is related to ISBA (Navascues et al., 2002).

The smallest resolvable scale of the model is contaminated by numerical noise. To prevent or minimize strong interaction between dynamics and physics on this scale, which can lead to numerical instability, a time step longer than the dynamic time step is taken in the physical parameterization calculations. The dynamic tendencies are averaged over the physic time step prior to their use in the physics calculations. As part of the postprocessing a number of useful meteorological parameters are calculated.

7.2 The DMI-HIRLAM system used in the SAT-MAP-CLIMATE project

The numerical experiments performed within the SAT-MAP-CLIMATE project (henceforth the SMC project) are based on modifications to the climate fields utilized in the operational DMI-HIRLAM system (DMI-HIRLAM). This model system is non-static with one to two updates on average per year to keep it in a state of the art shape as a highly competitive NWP system. The work on improving the NWP system is partly done within the HIRLAM community, which is a long-lasting cooperation between the Nordic countries, Ireland, Holland and Spain, established in 1985.

The SMC project utilized the version of DMI-HIRLAM that was operational at DMI in the summer of 2000 (Sass et al. 1999). This DMI-HIRLAM system uses non-linear normal mode initialization and Eulerian advection. All runs were made from analysis provided by the European Centre for Medium Range Weather Forecasts (ECMWF), which means that no HIRLAM data assimilation was performed. The forecasts were run on the DMI-HIRLAM-E grid (Figure 7-1) with a horizontal resolution of 0.15°×0.15° and with 31 levels in the vertical. In order to obtain an almost uniform horizontal resolution the model grid was rotated on the sphere with Equator running through the centre of the domain The model state on the lateral boundaries was specified by 6 hourly ECMWF analyses, with linear interpolation in time between the updates.

Treatment of surface processes (the focus of the SMC project) in DMI-HIRLAM is handled by two modules: A surface scheme and a turbulence parameterization scheme, respectively.

The surface scheme is fairly simple with three soil layers and three surface types (sea, land and ice). Each grid box contains information about fraction of land, sea and ice with solution of surface energy and moisture budget equations for each fraction. It is assumed in the budget calculations that the prognostic

variables in the grid column at the lowest model level (≈ 35 m) and above have the same values in each fraction. Furthermore, the sea surface temperature (SST) is kept constant during a forecast, but regularly updated by SST analyses from ECMWF.

The turbulence parameterization scheme is based on Cuxart et al. (1995) and Cuxart et al., 2000. It has turbulent kinetic energy (TKE) as a prognostic variable and parameterizes mixing length in terms of TKE and buoyancy. Further information about the schemes is given in Sass et al. (1999).

Of feasibility reasons the focus in the SMC project was on the local scale of Denmark. Accordingly, the modifications of the climate fields applied in the experiments have been restricted to Denmark and nearby surroundings. The climate fields utilized operationally have been modified by making direct or indirect use of satellite observations. The direct use of satellite data provided by the Advanced Very High Resolution Radiometer (AVHRR) on board the National Oceanic and Atmospheric Administration (NOAA) satellites concerns surface albedo and sea surface skin temperature (SST). The indirect use concerns the momentum roughness length z_0, which has been derived from land use maps (CORINE and AIS) by aggregation (up-scaling) in a two dimensional hydrodynamic model (Hasager and Jensen, 1999). In addition a leaf area index (LAI) field has been calculated from a normalized difference vegetation index (NDVI) derived from the AVHRR measurements (Bøgh et al., 2002a). Experiments have not been made with the LAI index included as a climate parameter, because the surface scheme in DMI-HIRLAM does not at present contain information about vegetation. It is planned in the next major upgrade of DMI-HIRLAM to include a more advanced surface scheme (ISBA) containing a number of vegetation types and with a related surface analysis and soil moisture assimilation package.

For most of the experiments the period from 15 April to 15 May 2000 has been selected. This period is considered to be particularly interesting for two reasons. The period has relatively large temporal changes in both albedo, SST and z_0 and it is optimal from a satellite measuring point of view by having nearly uninterrupted clear sky conditions over Denmark. The latter minimizes cloud contamination problems.

As a basis for the numerical experiments modified climate fields of albedo and SST based on NOAA AVHRR have been generated at five day intervals in the period from 15 April to 15 May 2000. In comparison the operational climate fields are updated monthly and smoothed in time by using a weighting function depending on the day of the month. For momentum roughness it has only been feasible to generate two modified roughness fields, one for winter and one for summer. In the operational system the z_0 fields are updated monthly and smoothed in time as described above.

A list of the numerical experiments performed in the SMC project is presented below. The name convention for the experiments are:

- NAL: Runs with modified albedo over Denmark.
- NST: Runs with modified SST in the Danish waters.
- NAS. Runs with modification of albedo and SST.

- NZ0: Runs with modified z_0 not including the effect of hedges.

- UZ0: Runs with modified z0 and the effect of hedges included.

- D15: Runs with operational climate fields, including a linear in time weighting of fields from adjacent months to avoid discontinuous changes from one month to the next. Further a model subroutine modifies the climate albedo. The latter includes a 9 point spatial smoothing.

- OPR: As D15, but without modification of the climate albedo field in the model.

The experiments NAL, NST, NAS, NZ0, OPR and UZ0 are run without time and space smoothing of the climate fields.

List of experiments

Date: 00042200,	experiments	NAL, NST, NAS, UZ0 and D15.
Date: 00042500,	experiments	NAL, NST, NAS, UZ0, D15 and OPR.
Date: 00042900,	experiments	NAL, NST, NAS, NZ0, UZ0, D15 and OPR.
Date: 00050400,	experiments	NAL, NST, NAS, UZ0, D15 and OPR.
Date: 00050900,	experiments	NAL, NST, NAS, NZ0, UZ0, D15 and OPR.
Date: 00051100,	experiments	NAL, NST, NAS, UZ0 and D15.
Date: 00051400,	experiments	NAL, NST, NAS, UZ0 and D15.
Date: 99120300,	experiment	UZ0 and D15.

In the list of experiments the starting date of the forecast is specified as yymmddhh, where hh is the initial hour, i.e. the starting hour (in UTC) of the forecast. The forecasts use lateral boundary files (analyses and forecasts) from the European Centre for Medium Range Weather Forecasts (ECMWF) with six hourly updates and linear interpolation in time in between. All the forecasts are run out to 24 hours with surface and near-surface variables written out in grib files every 3 hours from 06 UTC to 18 UTC

7.3 Albedo

A number of forecast experiments with the climate surface albedo over Denmark replaced by an albedo field derived from AVHRR data in 15 km × 15 km grid cells have been performed (see list in section 7-2). Figure 7-2 shows the typical impact of the modified albedo on the temperature at 2m height (T2m) measured as the difference in T2m between the operational (OPR) and the experimental forecast (NAL). The figure is typical in the sense that the absolute value of the differences in T2m between the operational forecast (OPR) and the experimental forecast (NAL) generally were less than 0.5 K in the performed experiments. These relatively small differences in T2m might indicate that accurate surface albedo is not a big issue in NWP and climate modelling. However, the forcing from an erroneous surface albedo is continuously present and does not only create a local temperature bias, but affects on the climate time scales the course of the atmospheric circulation. Consequently, due to local or regional errors in the surface albedo field, the model climate is likely to become different from the actual climate.

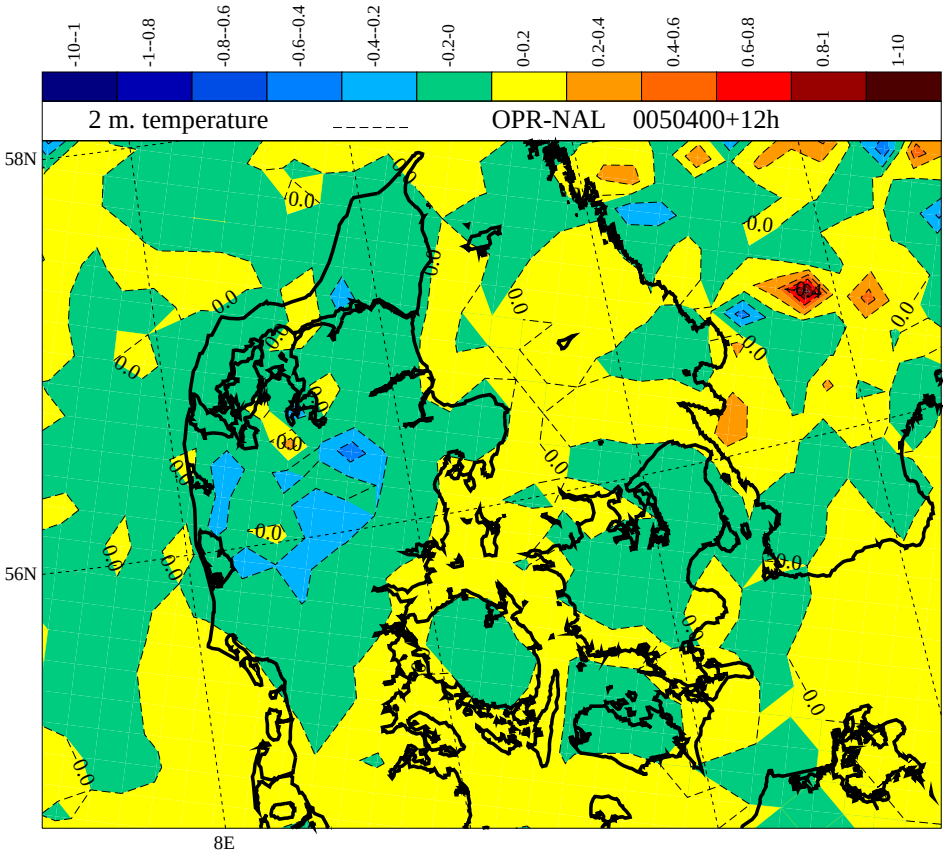

Figure 7-2. Twelve hour forecast of difference in 2m temperature (T2m) between the operational forecast (OPR) and the experimental forecast (NAL) valid at 12 UTC 4 May 2000. Contour (dashed line) interval is 0.2 K. Negative and positive differences are shown blue to green and yellow to red, respectively.

7.4 Sea surface temperature

Geometrically corrected and calibrated NOAA AVHRR data has been utilized to calculate the sea surface temperature (SST) in the Danish Waters. The derived SST's represent 5 day mean values. This procedure has been followed to obtain a good estimate of SST and at the same time minimizing problems with cloud contamination. The considered period is from 15 April to 15 May 2000. The split-window algorithm (Andersen, 1997) in Eq. (7-1) was used to calculate SST in °C.

$$SST = 1.0173 \cdot T_{c4} + 2.13959 \cdot (T_{c4} - T_{c5}) + 0.779706 \cdot (T_{c4} - T_{c5}) \cdot (\cos(vza)^{-1} - 1) - 278.43. \quad (7\text{-}1)$$

T_{c4} and T_{c5} are the radiometric calibrated surface temperatures (in K) of the two NOAA-14 thermal bands and vza is the view zenith angle of the satellite. Compared to the traditional split window algorithms (Price, 1984), the major modification consists of adding the correction term for the view angle.

A number of forecast experiments were run with and without the modified SST's in the Danish Waters (see list in section 7-2). Figure 7-3 shows the typi-

cal impact of the modified SST's. Substantial differences in *T2m* are seen over the Danish Waters and in coastal land regions.

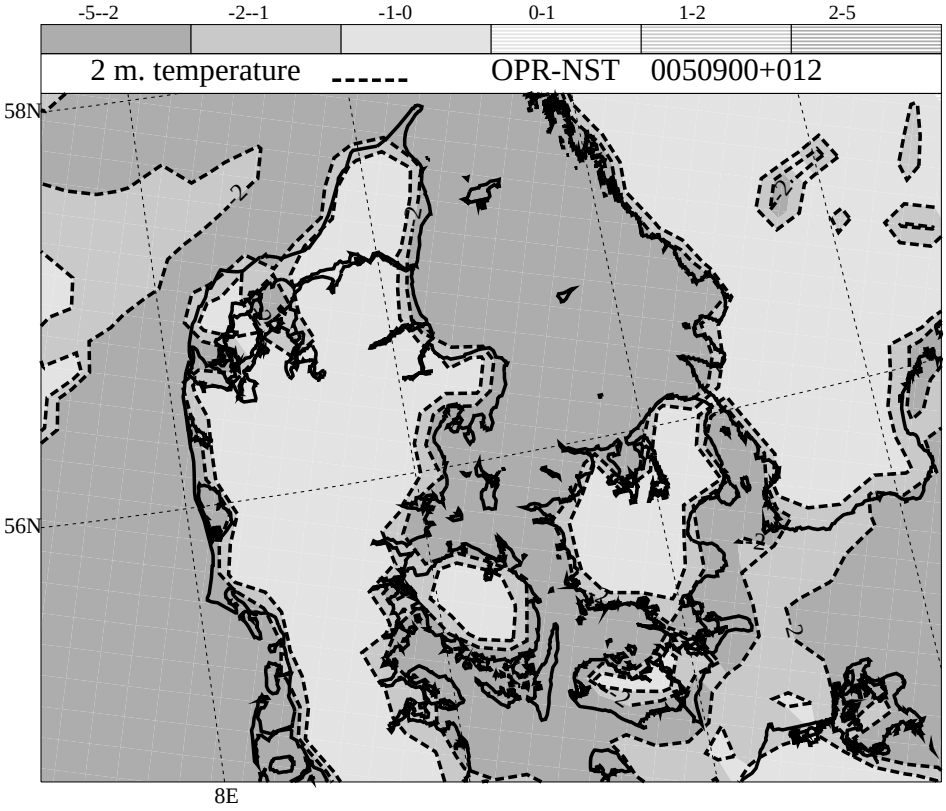

Figure 7-3. Twelve hour forecast of difference in T2m (dashed lines) between the operational forecast (OPR) and the experimental forecast with modified SST's (NST) valid at 12 UTC 4 May 2000. Contour interval is 1K . Negative differences are shaded.

Another example, comparing the predicted *T2m* over fractions of sea and land with observations, is shown in Figure 7-4. The observations (at 10m height) are from the off-shore site Vindeby. The predicted values are interpolated from the nearest model grid point to the site location.

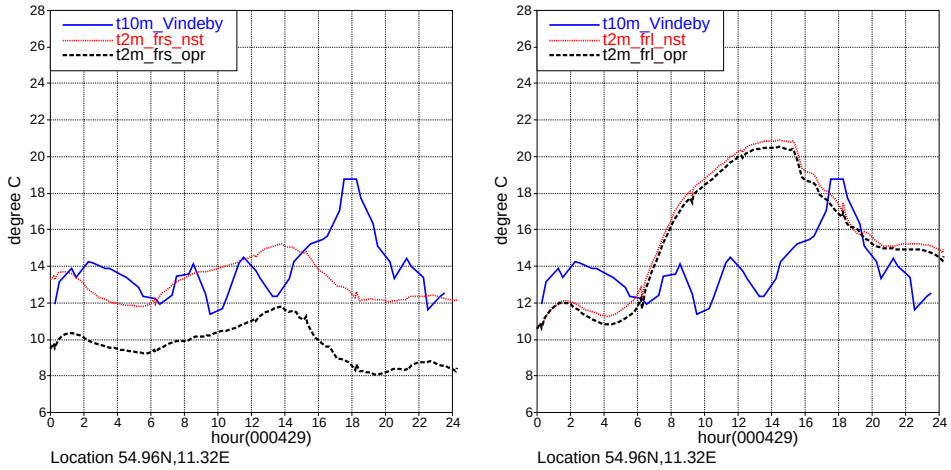

Figure 7-4. Observations of T10m at Vindeby 29 April 2000 compared with predicted T2m from model runs with modified SST (nst) and with operational SST (opr). Left and right: with predicted values over fraction of sea and land, respectively. Initial time of the model runs is 00 UTC 29 April 2000.Observations are collected by Risø.

The large impact seen in Figure 7-3 and Figure 7-4 is mainly due to a rapid and approximately linear in time increase of SST in the Danish Waters, as shown by Figure 7-5.

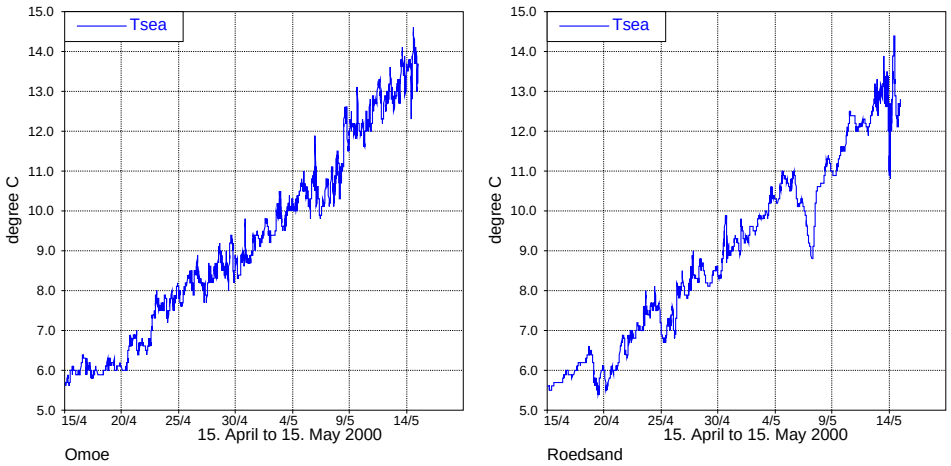

Figure 7-5. In situ SST measurements in Danish coastal waters at Omø (left) and Rødsand (right. Period: 00 UTC 15 April to 00 UTC 15 May 2000. Data kindly provided by SEAS.

The HIRLAM operational system uses a combination of a weighted average of adjacent monthly frozen climate SST's in the coastal waters and SST analyses from the European Centre for Medium Range Weather Forecasts (ECMWF) over open sea. The 5 day mean SST's derived from the NOAA AVHRR data seems much better than the operational procedure to be able to capture the observed rapid increase in SST. This is supported by the HIRLAM Spring-season verification scores of T2m for Denmark presented in Table 7-1. The Danish coastal stations have a substantial negative bias (indicating too cold coastal waters), while the land stations have a bias much closer to zero.

Table 7-1. The difference between HIRLAM predicted temperature and observed at 2 m.Period: April-June.

	Coastal	Coastal	Land	Land
Year	Bias (^{o}C)	Rms (^{o}C)	Bias (^{o}C)	Rms (^{o}C)
1998	-1.1	2.0	-0.7	1.8
1999	-1.1	1.7	-0.5	1.7
2000	-1.5	2.1	-0.3	1.8
2001	-0.8	1.8	0.2	1.9

A four-dimensional variational data assimilation system (Huang et al., 2002) under development in HIRLAM makes future almost real time use of meteorological data derived from satellite measurements feasible. The results presented here indicate that significant improvement of T2m (particularly in coastal waters) can be obtained by extensive use of `high resolution in time' SST's derived from satellite measurements.

7.5 Momentum roughness

The vegetation roughness field in operational use is generated by assigning typical roughness values to a number of land use classes. The annual cycle in the field is taken into account by assigning monthly values.

In the SMC project two z_0-fields, one for summer and one for winter, have been calculated by aggregation (up-scaling). The aggregation involves a 2-dimensional hydrodynamic model (Hasager and Jensen, 1999). This model takes as input local z_0 values on satellite pixel scale, and the output of the model is grid-cell average (here approximately 15 km × 15 km) friction velocity $<u_*>$ and the corresponding effective roughness length $<z_0>$. It is assumed that $<u_*>$ and $<z_0>$ are related by the logarithmic wind law.

The Earth Observation (EO) satellite data is used in a land cover type classification of each pixel. Typical z_0 values for each land cover type are then used to create a map of local roughness on the pixel scale used as input to the aggregation model (for details see Hasager et al., 2002c). Note that the aggregation technique handles only the roughness variation due to land cover types, not the orography roughness. The latter is an important issue in a more hilly terrain than the Danish. The aggregated z_0 does not contain information about roughness in urban grid cells. This information has been merged into the aggregated field from the roughness map in operational use. It was found that the aggregated values generally were smaller than those derived from measurements, particularly in summer. It was suspected that the discrepancy to some extend could be due to the effect hedges. Roughness of hedges is not taken into account in the local z_0–field based on the land cover types. Inclusion of the roughness effect of hedges resulted in a much better agreement between the aggregated and measured $<z_0>$ (Hasager et al., 2002c).

A number of numerical experiments have been performed with z_0-fields derived by aggregation from the Land Cover Map Plus Areal Information System (AIS) and including the effect of hedges.

Two cases are presented below. The first case (3 December 1999) has near-surface wind speeds between 20 and 25 ms^{-1} over the southern part of Denmark.

The second case (29 April 2000) has clear sky conditions and much weaker wind speeds with a superposed sea-breeze circulation. The reason for choosing these cases are firstly that they represent widely different wind regimes with near-neutral stability in the first case and a diurnally varying stability in the second case. Secondly, they contain impact studies of the modified roughness field for both winter and summer. Thirdly, the spring case has low synoptic scale forecast uncertainty due to an almost stationary synoptic weather pattern. A drawback of the winter case is on the other hand a relatively high forecast uncertainty due to rapidly changing weather conditions, which makes evaluation against observations of little use. The focus has therefore been on the impact of the modified roughness field on the near-surface winds, rather than to answer the question whether they improve the wind forecasts or not. Only hints can be given about this.

For the December case the difference in mean wind speed at 10m height between the operational forecast (D15) and experimental forecast (UZ0) with the aggregated roughness field (includig the effect of hedges) is shown in Figure 7-6a. The impact is as expected with a clear negative correlation between the difference in wind speed Figure 7-6a) and the corresponding difference in rougnness (operational minus experimental) shown inFigure 7-6 b. The aggregated roughness map (UZ0) for winter contains both regions with higher and lower roughness than in the operational field (D15). Due to significant forecast errors in both phase and intensity of the surface cyclone (shown by closed sea level isobars in Figure 7-6a an evaluation of the forecasted winds against observations does not show whether the aggregated roughness field is actually an improvement. However, a hint can be obtained form the second case.

The difference in wind speed and roughness for the April case is shown in Figure 7-6c and d, respectively. Again a negative correlation is seen between the difference fields of wind speed and roughness. The effect of hedges on the summer season aggregated roughness is seen in Figure 7-6d. In major parts of Denmark, and particularly in Jutland, where the hedge density is generally higher than in the eastern part of the country, the aggregated roughness is higher than in the operational roughness map. Figure 7-6c shows th 10m wind speed difference in a 15 hour forecast valid at 15 UTC 29 April 2000. The pattern is similar for other valid hours on 29 April and for other forecast initial times in the considered period from 15 April to 15 May (figures not shown).

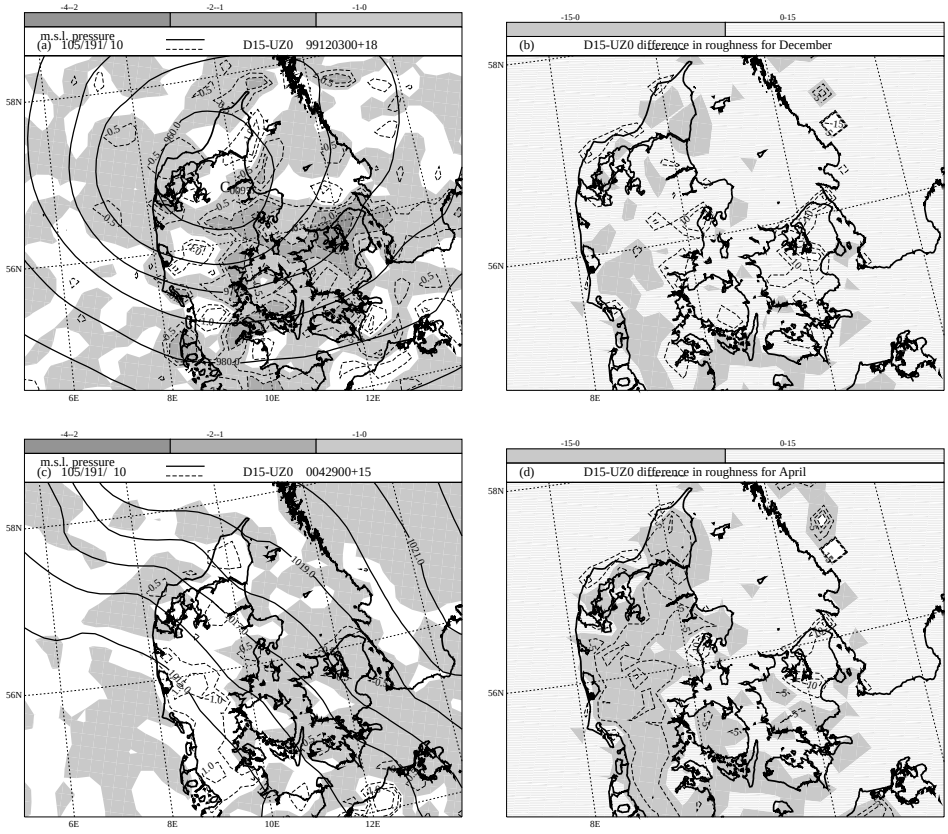

Figure 7-6. Left column: Sea level pressure for D15 (full lines, interval 5 hPa in (a) and 1hPa in (c)) and difference in wind speed at 10m height (dashed lines, contours -2,-1,-0.5,0.5,1,2 ms^{-1}, and negative difference shaded). In (a) 18h forecast valid 18 UTC 3 December 1999, in (c) 15h forecast valid 15 UTC 29 April 2000. Right column: Difference in roughness (dashed lines, contour interval 5 cm, and negative differences shaded) between D15 and UZ0, in (b) for December and in (d) for April.

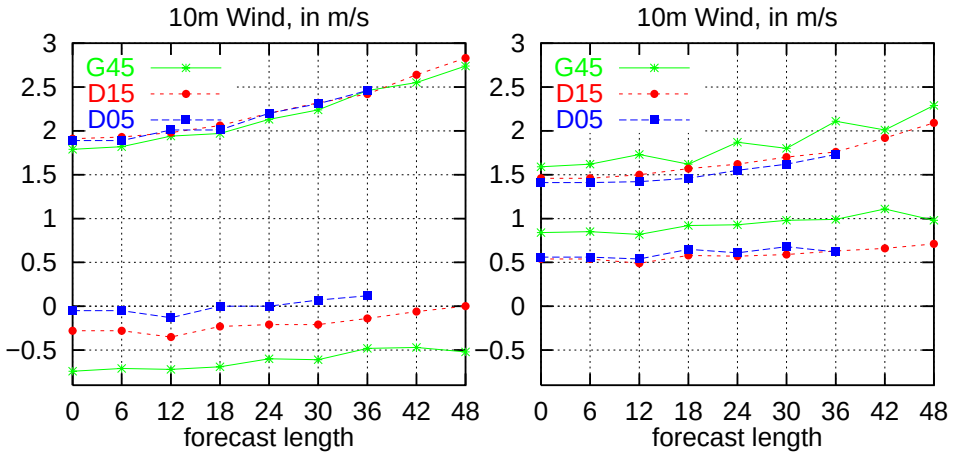

Figure 7-7. Verification results for the second quarter of 2000 (bias and std.dev.) for 11 coastal stations (left) and 11 land stations (right) in Denmark for model versions DMI-HIRLAM-G (G45), DMI-HIRLAM-E (D15) and DMI-HIRLAM-D (D05). The numbers correspond roughly to the horizontal model resolution in km. All model versions have 31 levels in the vertical.

A routine verification for the second quarter of 2000 af 10m wind speed predicted by the operational DMI-HIRLAM model system against observed wind speed at a number of Danish land and coastal stations is shown in Figure 7-7. The figure shows that the predicted wind speeds over land are too high (about 0.5 ms^{-1} for D15). For summer it has been shown that the introduction of an aggregated roughness with inclusion of the effect of hedges tends to reduce the forecasted 10m wind speed over land (Figure 7-6c). This indicates, but does not prove that in summer a replacement of the operational roughness map with a map of aggregated roughness will reduce the systematic forecast error (bias) of 10m wind speed over land. A proof of this hypothesis requires for both winter and summer parallel runs of the forecasting system over periods of several months. However, this has been outside the scope of the present project.

8 Multi-year impact study in the HIRHAM climate model

Predicting longer-term climatic trends will have to be based on another model than the operational HIRLAM model, because this model is developed specifically with the objective to produce high quality short-term forecasts. On climate scales, several of the physical parameterisations are inadequately treated and hence the performance of the model deteriorates when integrated beyond weeks (Sass and Christensen, 1995). In stead we have utilized the DMI climate version HIRHAM4 (Christensen *et al*., 1996) for this purpose. Moreover, it is essential to evaluate the effect of introducing seasonality not only for a small region such as defined by Denmark, in order to assess any climatic impact. Experiments where the introduction of seasonally varying surface characteristic fields, have therefore been carried out for a wider European domain, and the data source used to introduce these new variables differ from those adopted in the rest of the present study. Christensen et al. (2001) provide a thorough discussion of the fields in concern. Furthermore, not only roughness length and albedo are considered.

8.1 HIRHAM performance over Europe

15 year E50 control run

Several 15-year baseline simulations with initial and lateral boundary conditions as well as SST and sea ice conditions from the European Centre for Medium-Range Weather Forecasts (ECMWF) re-analysis product (ERA), thoroughly described in Gibson *et al*., (1997), has been conducted with the aim to construct an improved version of the HIRHAM4 model. The model used in the *Regionalization of Anthropogenic Climate Change Simulations (RACCS)* project (e.g. Machenhauer *et al*., 1998; hereafter RACCS) is originally based on the dynamical core and physiographic database of the HIRLAM level 2 system (Gustafsson, 1993) and the physical parameterisations of the ECHAM4 model (Roeckner *et al.*, 1996). This model is documented in Christensen *et al.* (1996).

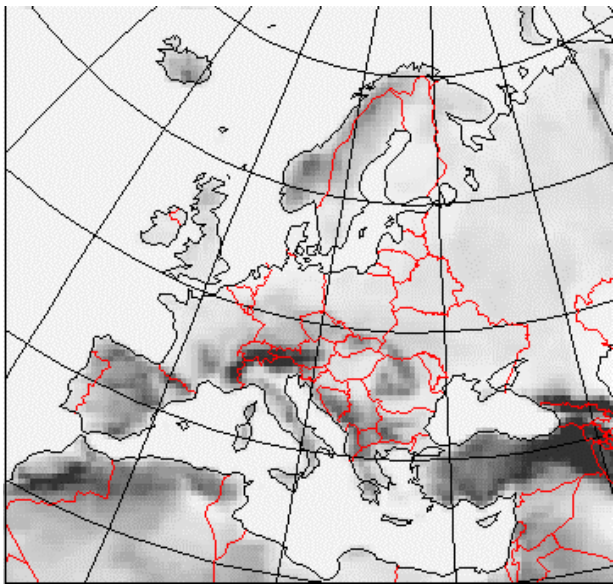

Figure 8-1. European reference domain; 110 × 104 grid points at 50 km resolutiom

In order to have a baseline simulation for validation of possible model improvements, a control experiment was conducted using the old 'standard' HIRHAM version, hereafter denoted E50. The 15 years of ERA have been used to force HIRHAM4 over a region as outlined in Figure 8-1. The computational grid utilizes a rotated latitude-longitude coordinate system, with the coordinates of the rotated South Pole at 27°E, 37°S, whereby the rotated equator crosses the middle of the computational domain minimizing projection effects. The model grid has a mesh of 110 by 104 points with a horizontal resolution of 0.44° times 0.44° (approximately 50 km). The vertical discretization consists of 19 irregularly spaced levels in hybrid σ-p coordinates from the surface up to 10 hPa with 5 vertical layers in the planetary boundary layer. The model time step was 300 seconds. At the lateral and lower (over sea only) boundaries HIRHAM4 was forced by the data from ERA. The resulting climatology has been compared to two verification data sets. The atmospheric fields (i.e. mean sea level pressure and 500 hPa geopotential heights) have been compared to the ERA data themselves (not documented in here), while surface parameters are compared with the gridded CRU (Hulme *et al*., 1995) climatology of the various fields. In the present work we only used the CRU data from the period 1979-1993 for surface air temperature and precipitation in the analysis.

Figure 8-2 displays the temperature and precipitation biases with respect to the CRU data set for summer and winter - any reference given below to the bias in other seasons are not illustrated. The major findings from the validation of the reference run, E50, which can be assessed as significant model biases, can be summarised as follows:

- The model simulates too much precipitation over Northern Europe throughout the year, except during summer.
- The summer time precipitation is too low over Central and Southeastern Europe.
- The precipitation is generally simulated too low around the Mediterranean Sea throughout the year, most pronounced in summer and autumn.

- A cold bias is seen over most of Europe during spring.
- A warm bias is seen over most of Europe, strongest for Southern and Southeastern Europe, during summer.
- Over Scandinavia a cold bias is observed throughout the year, except during winter, where a warm bias is present.

Most of these findings can be related to systematic errors in the simulated flow within the model domain. The same explanations as put forward in RACCS (see also Christensen *et al*., 1998) seem to be adequate to explain several of the biases seen in both precipitation and temperature here. However, in the present simulation the biases in the flow pattern remain relatively small in comparison, simply because the driving conditions are observations, while RACCS used output from general circulation models. Therefore the connection between flow errors and temperature and precipitation biases are less obvious. This will be emphasised when the new reference version of the model will be discussed.

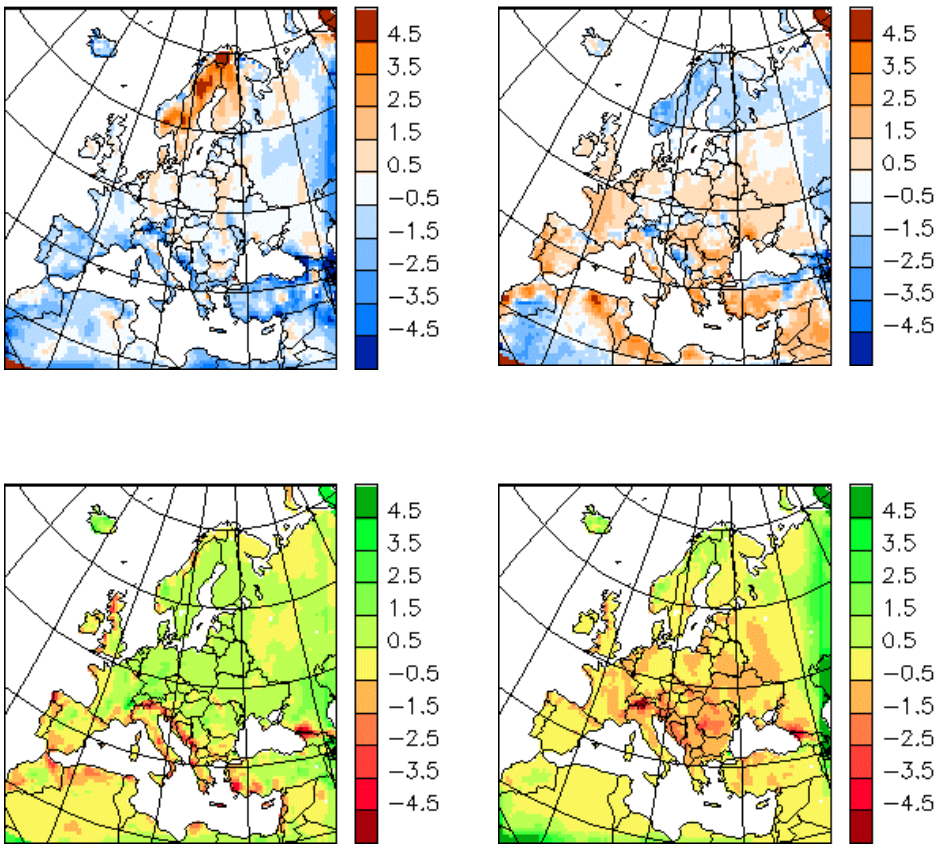

Figure 8-2. Seasonal biases (Left: winter; Right: summer) for the control run E50: ***Upper row*** *surface air temperature bias in ºC and* ***lower row*** *precipitation bias in mm/day.*

8.2 Main model changes

15 year F50 new reference model version

Much effort went into updating the part of the model, which generates the so-called climate fields. These constitute parameters essential for the model, but not calculated as part of the governing equations. Examples are those of orography, vegetation coverage and albedo. New global data sets at very-high resolution (notably 1 by 1 km) became available for such an enterprise only recently. Hagemann *et al*. (1999) and Christensen *et al*. (2001) describe in detail how the new data sets have been processed and compare the old and new resulting fields used in the European 50 km version of HIRHAM4. It has been seen in year-long[3] simulations, that the combined effect of adding all changes were generally to the better, but mainly due to the changes in the soil water holding capacity. Furthermore, the dominating part of the roughness length is due to orographic variances, an issue, which is still very crudely treated in most models, and most likely also in HIRHAM. Also, it was seen that introducing the new fields had very little impact on the wintertime performance of the model. It was evident that an improved performance over southern Europe was demonstrated, but that the introduced changes could not completely eliminate the systematic biases observed in the E50 simulation. In particular, the tendency to be too dry and to warm during summer in the southern part of the domain was still present, albeit somewhat reduced. Similarly, in the central and northern part of the model domain, substantial positive precipitation bias remained.

Modifications to the physical parameterisation have therefore also been introduced, all with the aim to increase summer time precipitation in the South in general and to reduce precipitation in the central and northern part of the domain. This involved several steps: evaporation of precipitation below clouds was reduced, convective cloud cover was made more favourable in that the relative humidity profile for saturation was modified, and auto conversion rate from specific humidity to rain drops within convective clouds was substantially increased. Analysis of the frequency distribution of the E50 simulations indicated that for northern Europe, and Denmark in particular, the model had far too few dry days. In order to deal with that, a modification introducing a threshold value for formed precipitation within a layer to fall out was introduced. Later on this threshold was made dependent on whether or not convection was going on. In this case the threshold was avoided.

3 Even one-year long simulations cannot be considered to provide statistically significant validation estimates; decadal simulations appear to be necessary (Machenhauer *et al*., 1998).

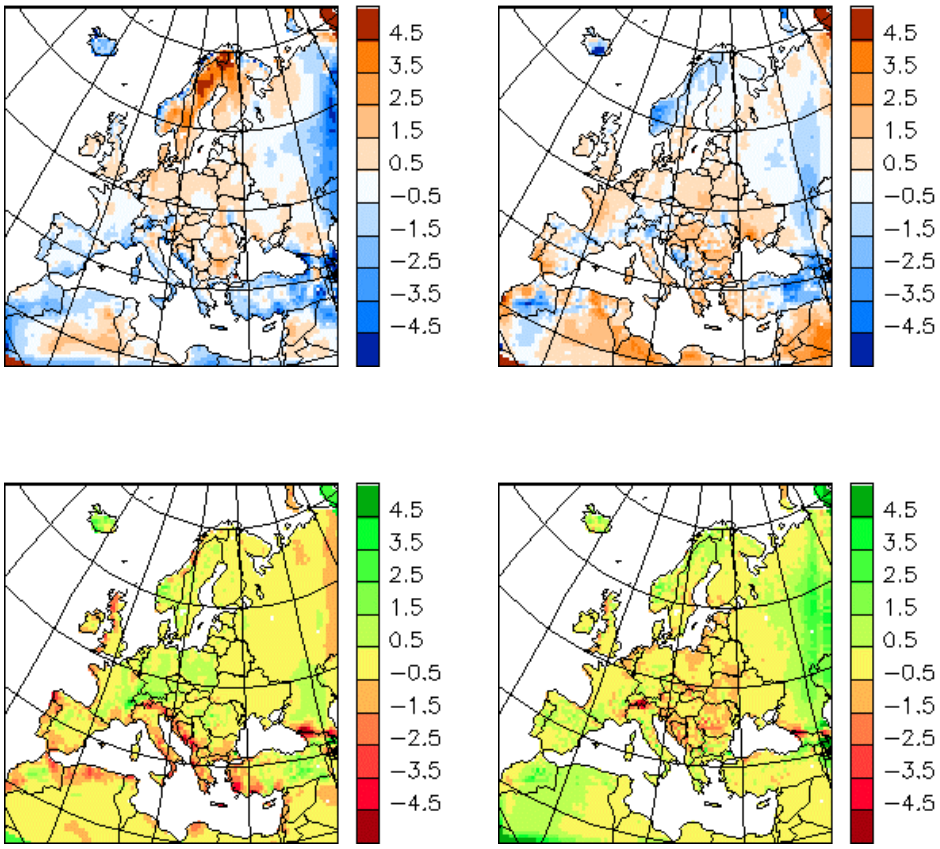

Figure 8-3. Seasonal biases (Left: winter; Right: summer) for the improved model run F50: ***Upper row*** *surface air temperature bias in ºC and* ***lower row*** *precipitation bias in mm/day.*

In the following the combined effects from all the approved changes are discussed. Major improvements regarding the simulation of present day mean climate conditions both regarding temperature and precipitation has emerged. First and foremost, the precipitation in central and northern Europe is now very close to observed conditions, throughout the year. Also, summertime precipitation in southern Europe is greatly improved, although still too low. Temperatures are moderately improved, but they were already within a few degrees from observed values over large parts of the region. An important result of the analysis of the new model run, hereafter denoted as F50, is that only very minor changes occur in the systematic error of the mean flow in all seasons (not shown).

Figure 8-3 illustrates the improvements made during both summer and winter in terms of temperature and precipitation biases, e.g. to be compared with Figure 8-2. Despite the obvious improvements, there are still unresolved biases, which the present set of improvements cannot account for. In summary these are:

- The model still has a positive precipitation bias in the north, but confined to winter and spring, but substantially reduced in comparison to E50.

- The summer time precipitation is still too low over parts of Central and Southeastern Europe, but over much less of the domain than previous. A positive precipitation bias has emerged over the Iberian Peninsula.
- The precipitation is simulated too low around the Mediterranean Sea, but now mainly confined to the autumn and winter season.
- A weak warm bias is present over most of Europe in spring, more severe near the Black Sea.
- A warm bias is present over Scandinavia during winter.

As the flow bias is very similar to the E50 simulation in all seasons, we ascribe the entire model improvements to the introduction of the new climate fields and the modifications made to the physics. Therefore, it is tentative to suggest that climate models in general and regional model in particular are sensitive to the specific treatment of surface-atmosphere interactions. Moreover, it seems that with more realistic representation of surface and sub-surface characteristics, the ability to simulate present day conditions is substantially improved when compared to more rudimentary methods, like not allowing important parameters such as albedo, roughness length (which is actually not varying in the F50 experiment) and leaf area index, to change annually.

9 Conclusion

The overall goal of integrating Earth Observation (EO) data as surface boundary conditions in the HIRLAM weather prediction model and the HIRHAM regional climate model for impact assessment of land surface processes to weather forecasting and climate prediction is fullfilled.

More specifically a succesful use of satellite maps of albedo, sea and land surface temperatures, vegetation parameters, net radiance balance and land cover classes is demonstrated in part for the HIRLAM model, the HIRHAM model and for direct evapotranspiration estimation.

- *Albedo maps* from NOAA AVHRR show to be very similar to the climatological maps operationally used in the HIRLAM model, hence the effect of using the new satellite-based albedo maps is only minor. For the HIRHAM model even a slightly different albedo may have importance in the radiation balance and hence for the ability to simulate present day conditions as well as climate change. It is tested at regional scale.

- *Sea surface temperature maps* from NOAA AVHRR show to be different from the climatological maps operationally used in the HIRLAM model, and the effect of using the new satellite-based sea surface temperature maps is significant. The land-sea breeze is better modelled with the new input.

- *Roughness maps* based on the land cover class map AIS (Danish Areal Information System, 2001) derived from Landsat TM satellite images and hedge density estimated from the digital TOP10DK map (National Cadastre and Survey, 1995-2000) are obtained by assigning local roughness values per class. The roughness maps are used as input for a

microscale aggregation model and the model results are effective momentum roughness values for the HIRLAM grid cells at 15 km by 15 km grid for summer and winter conditions. Generally, the new maps have a higher roughness than those used operationally in the HIRLAM model and the effect of using the new maps is that a positive bias in wind speed over land is reduced during spring.

- *Vegetation parameter maps* of LAI (leaf area index) and NDVI (Normalized Difference Vegetation Index) are obtained from NOAA AVHRR and Landsat TM and used in a direct method for the estimation of evapotranspiration as well as in a method for calculating effective scalar roughness values.

- *Net radiation balance maps* from NOAA AVHRR are obtained from the global albedo and brightness temperatures. The net radiation balance maps are used in a direct method for the estimation of evapotranspiration.

- *Evapotranspiration maps* from NOAA AVHRR are estimated from a method integrating the net radiation balance, the soil heat flux assesed through NDVI and the radiation extinction by the canopy and the sensible and latent heat fluxes found from an empirical equation for the vapour pressure at the surface and the corresponding atmospheric resistance, surface resistance and evapotranspiration rates.

Other important findings within the SAT-MAP-CLIMATE project are on improved atmospheric correction of satellite images, the added roughness of hedges, the aggregation of effective scalar roughness lengths and the importance of surface-atmosphere interactions for regional climate modelling.

- *An improved atmospheric correction* of NOAA AVHRR satellite images is obtained. It is demonstrated that the predicted weather conditions at 12 GMT on air temperature and air humidity from the HIRLAM weather forecast model are adequate proxies for the air temperature and air humidity at the time of the NOAA AVHRR satellite passage at 12.30 to 15.00 GMT. This means that the atmospheric correction of the NOAA AVHRR satellite images is improved by using these values instead of e.g. thermal remote sensing estimates of air temperature and microwave remote sensing of air humidity.

- *The added roughness effect of hedges* to the total momentum flux are described from theory and from statistical information on hedges in Denmark as well as quantified from meteorological observations from tall masts at different sites through several years. A practical method of adding roughness as a function of hedge density per grid cell is applied.

- *Effective scalar roughness values* are calculated through a new version of the microscale aggregation model. In the first model version it is crudely assumed that a constant ratio between the momentum and scalar roughnesses exists. In the new version the scalar roughness is modelled as a function of land cover type and leaf area index and their covariations in the landscape. The local roughness value for momentum for water is a function of wind speed (Charnock's relation). For all

other land cover classes roughness values from experiments and literature are assigned to satellite-based land cover maps. The land and sea surface temperatures used are the radiant temperature from thermal remote sensing. It is found that in heterogeneous terrain, the effective scalar roughness length is much smaller than one tenth of the effective roughness for momentum. In other words, it is found that kB^{-1} typically is much larger than the classical value of 2.3, e.g. 5.2 for a Danish summer case in Foulum.

- *Surface-atmosphere interactions in regional climate modelling* are important issues. It is demonstrated at the European scale with the HIRHAM model, that the introduction of more realistic representations of surface and sub-surface characteristics improve the ability to simulate present day conditions. The input surface parameters are albedo, roughness including orography and leaf area index. Major improvements have emerged regarding the simulation of present day mean climate conditions of temperature and precipitation and this is fundamental for accurate and reliable climate predictions.

10 Future perspectives

The basic methodology of the SAT-MAP-CLIMATE project is combining physical descriptions of the surface processes and mapping of land and sea surface characteristics by Earth Observation (EO) data from satellite remote sensing.

It is possible to apply this methodology for a range of atmospheric, climatological, hydrological and agro-meteorological purposes. In very close connection to the achieved results, it is foreseen that as the grid cells of weather prediction models decrease towards a size of eg 1 km by 1 km, the need for accurate effective roughnesses will be imperative. This will include the directional effect of roughness changes where for instance offshore and onshore flow has a very different turbulent response. Further may atmospheric stability effects be included.

A future perspective would be to map the possible changes in the Danish land cover, eg is a substantial increase in re-forestation foreseen in the coming 20 years. This will dramatically increase the effective roughness and hence may have implications for the long-term climatic trends in Denmark. It may therefore be important to include it in regional climate prediction modelling. Another related issue is an improved parametrization for roughness related to orography, which has great importance in regional climate modelling.

There is an increasing concern within the European community regarding the water resources. Given the strong interaction spatially and vertically this has led to a proposal within EU of subdividing Europe into large water management units (smallest size=Sjælland). Based on the outlined methodology, the water vapour flux into the atmosphere could be monitored with an appropriate resolution in both time and space from high-resolution mesoscale models as the DMI-HIRLAM-D05. In this way a perfect tool for monitoring the most import sinks for the water resource in Europe, namely the evapotranspiration, could be developed.

The new effective roughness length for scalars obtained within the SAT-MAP-CLIMATE project, is a break-through within a physically-based parameterisation of the parameter. However, a validation study is needed prior to applying it at a near-operational level. It is foreseen that the validation study will involve a number of sites with variable land cover, leaf area and roughness.

Projects similar to the SAT-MAP-CLIMATE project will most certainly be proposed within the forthcoming sixth framework programme of the European Commission (EC). Through the SAT-MAP-CLIMATE project experiences and results, we seem to be well prepared for further international participation in related work.

At European level it can be mentioned that we currently participate in Expressions of Interest (EoI) to the EC, among those eg

- ASOLPIC ("Advanced Satellite Observation of Land Processes and Interactions with Climate")
- ATMOS ("Atmospheric boundary layers over heterogeneous terrain: methods for applied use").

At the Nordic level, two proposals are submitted and the methodology may be further utilized in Nordic cooperations within the proposed

- "Microclimate Science Center" for a Nordic Center of Excellence.
- " Nordic Graduate School of Microclimate Science" (NorFA)

At the national scale in Denmark parts of the results from the SAT-MAP-CLIMATE project may benefit current projects such as the

- EO-FLUX-BUDGET acronym for Earth Observation data for upscaling carbon FLUX and water BUDGET at Zealand, years 2001-2004[4]
- RS-model indlejring acronym for Remote Sensing based Crop Simulation and Soil-Vegetation-Atmosphere-Transport modelling - continuation (indlejring), years 2001-2005[5].

A direct involvement in future remote sensing missions is considered of great importance in order to secure optimal EO data for the specific purposes treated within the SAT-MAP-CLIMATE project. A direct involvement is already achieved as some SAT-MAP-CLIMATE participants are associate scientists within two major European EO missions

- SPECTRA: the ESA mission: "Surface Processes and Ecosystems Changes Through Response Analysis" mission that is currently in Phase A, ie among the three possible missions out of which two are scheduled to be launched in 2008/2010 (Earth Observation Quarterly, 2002)
- RHEA: the CNES (French Space Agency) Earth Observation proposal: RHEA "A micro-satellite mission for the study and modeling of land surfaces" for year 2004-[6].

Further is a direct connection to ongoing work in

- European SAF (Satellite Application Facility) projects obtained[7].

4 EO-FLUX-BUDGET http://www.geogr.ku.dk/research/eoflux/

5 RS-model indlejring http://www.risoe.dk/vea-atu/rs/RS-model/

6 RHEA http://www.uv.es/ucg/symposium/PROfINAL.pdf, Presentation S11.2

7 SAF http://www.eumetsat.de/en/index.html?area=left4.html&body=/en/area4/saf/internet/&a=430&b=1&c=400&d=400&e=0

It is foreseen that an in-depth and up-to-date knowledge on EO data is sustained through the partners active participation in these different international and national networks and initiatives.

It seems compelling to maintain a strong Danish involvement in applied EO sciences as the amount of EO data is increasing rapidly and society's demand for reliable predictions on weather, climate and other environmental factors is high. Only by effectively utilizing the new EO products, may we obtain optimal results for our society.

It is our hope that Danish EO "know-how" will be given high priority for the benefits of applied research and monitoring purposes within Denmark.

11 Acknowledgements

Funding from the Danish Research Agency, Space Research (ESA-følgeforskning) Sagsnr. 5006-00-0063 for the SAT-MAP-CLIMATE project is greatly acknowledged. Part of the work on improvements of the HIRHAM model was supported by the 5th Framework Program of the European Union (project MERCURE, contract No. ENV4-CT97-0485). Observations from Foulum were collected in the RS-model project, now continued in the RS-model indlejring. The observations from Rødsand and Omø are from SEAS and the observations from Horns Rev from ELSAM/ELTRA (Techwise). Charlotte Hasager is very thankful to VITO and the SAR Scape project for the invitation to present in the workshop and the travel costs. The spin-off work in Alpilles with Albert Olioso in France relates to the 5th Framework Program of the European Union contract WATERMED project (ICA3-CT-1999-00015). We thank Bjarne Fog from Institute of Geography (IGUC) for help on the GIS-vector analysis, Jens V. Olsen for programming software.

12 References

Andersen, H. S. (1997). Land surface temperature estimation based on NOAA-AVHRR data during the HAPEX-Sahel experiment. J. Hydrol. 188-189: 788-814.

Batchvarova, E., Gryning, S. E., and Hasager, C. B.: 2001, 'Regional Fluxes of Momentum and Sensible Heat Over a Sub-Arctic Landscape During Late Winter', *Boundary-Layer Meteorology* 99, 489-507

Boegh, E., Schelde, K. and Soegaard, H. (2000). Estimating transpiration rates in a Danish agricultural area using Landsat Thermal Mapper data. Physics and Chemistry of the Earth 25(7-8): 685-689.

Boegh, E., Soegaard, H. and Thomsen, A. (2002a). Evaluating evapotranspiration rates and surface conditions using Landsat TM to estimate atmospheric resistance and surface conditions. Remote Sensing of Environment 79: 329-343.

Boegh, E., Soegaard, H., Christensen, J. H., Hasager, C. B., Jensen, N. O., Nielsen, N. W. and Rasmussen, M. S. (2002b). Combining weather predictions and remote sensing data for the calculation of evapotranspiration rates in Denmark. International Journal of Remote Sensing, *submitted*.

Bradley.E.F.: 1968, 'A Micrometeorological Study of Velocity Profiles and Surface Drag in the Region Modified by a Change in Surface Roughness', *Quarterly Journal of the Royal Meteorological Society* **94**, 361-378

Carlson T., O.Taconet, A.Vidal, S.Moran and R.Gillies (eds.), 1993, Thermal remote sensing of the nergy and water balance over vegetation in conjunction with other sensors, La Londe Les Maures, 20-23 Sep. 1993, pp330

Charnock, H. 1955 Wind stress on a water surface. *Quart. J. Royal Met. Soc.*, 81, 639-640

Christensen, J.H., O.B. Christensen, P. Lopez, E. van Meijgaard, and M. Botzet, 1996: The HIRHAM4 Regional Atmospheric Climate Model. DMI Scientific Report 96-4.

Christensen, J.H., O.B. Christensen, J.-P. Schulz, S. Hagemann and M. Botzet, 2001: High resolution physiographic data set for HIRHAM4: An application to a 50 km horizontal resolution domain covering Europe. DMI Technical Report 01-15.

Christensen O.B., J.H. Christensen, B. Machenhauer and M. Botzet, 1998: Very high-resolution regional climate simulations over Scandinavia – Present climate, J. Clim., 11, 3204-3229.

Cuxart, J., Bogeault, P. and Redelsperger, J. L., 1995. Turbulence closure for a non-hydrostatic model. *In 12th AMS symp. On Boundary Layer Turbulence,* pp. 409-412.

Cuxart, J., Bogeault, P. and Redelsperger, J. L., 2000. A turbulence scheme allowing for meso-scale and large-eddy simulations. *Quart. J. Roy. Meteorol. Soc.*, 126, 1-30.

Czajkowski, K. P., Goward, S. N., Shirey, D. and Walz, A. (2002). Thermal remote sensing of near-surface water vapour. Remote Sensing of Environment 79: 253-265.

Danish Areal Information System (2001) AIS map 1:25.000, 2000 See http://www.dmu.dk/1_viden/2_miljoe-tilstand/3_samfund/ais/index_en.htm

Dellwik, E. and Jensen, N. O.: 2000, 'Internal Equilibrium Layer Growth Over Forest', *Theoretical and Applied Climatology* **66**, 173-184

EEA, 1992 CORINE land cover. A European Community project, European Enviroment Agency Task-Froce, Directorate General for the Environment, Nuclear Safety and Civil Protection. Commission of the European Communities. Earth Observation Quarterly, 2002, *Earth Observation Quarterly,* **No 70**, p 3

Garratt, J.R. 1992. The atmospheric boundary layer. Cambridge Atmospheric and Space Science Series, page 102. 316pp

Garratt J.R. and B.B. Hicks (1973) Momentum heat and water vapour transfer to and from natural and artificial surfaces. *Q.J.R.Met.Soc*, **99**, 680-687.

Gibson, J.K., P. Kållberg, S. Uppala, A. Nomura, A. Hernadex and E. Serano, 1997: ERA Description. ECMWF Re-Analysis Project Report Series 1

Gleick, J., 1987, Chaos. Making a new science, Penguin Books, NY, pp352

Gustafsson, N., 1993: HIRLAM 2 final report. HIRLAM Tech. Report No. 9, 126pp.

Hagemann, S., M. Botzet., L. Dümenil, and B. Machenhauer, 1999: Derivation of global GCM boundary conditions from 1km land use satellite data. MPI Report No. 289, Max-Planck-Institute, Hamburg.

Hasager C.B. 1997. Surface fluxes in heterogeneous landscape. *Ph.D. dissertation. Risø-R-922*(EN), 177p

Hasager, C.B. & Jensen, N.O.1999 Surface-flux aggregation in heterogeneous terrain, *Quart. J. Roy. Met. Soc.* **125**, 2075-2102.

Hasager, C.B., S.E. Gryning, E. Batchvarova and N.O. Jensen, 2000, Regional fluxes over a high latitude boreal landscape. EGS 2000, 25. General assembly: Millennium conference on earth, planetary and solar systems sciences, Nice (FR), 25-29 Apr 2000. *Geophys. Res. Abstr.* (CD-ROM) (2000) **2** http://www.copernicus.org/EGS/egsga/nice00/programme/abstracts/aac4964.pdf

Hasager, C.B., Jensen, N.O., Boegh, E., Soegaard, H., Schelde, K. & Thomsen, A., 2001. Scaling-up evapotranspiration from field to regional scale based on optical remote sensing scenes. In the *Proceedings of symposium Remote Sensing and Hydrology 2000*, Santa Fe, New Mexico, USA, April 2000. IAHS Publ. No. 267, 292-295

Hasager, C. B., Nielsen, N. W., Jensen, N. O., Christensen, J. H., Dellwik, E., Soegaard, H., and Boegh, E.: 2002c, 'Effective Roughness Calculated From Satellite-Derived Land Cover Maps and Hedge Information and Used in a Weather Forecasting Model.', *Boundary-Layer Meteorology* (submitted)

Hasager, C.B.; Olioso, A.; Jacob, F., 2002a Parametrisation of aggregated roughness and sensible heat flux from field scale to hydrological scale by microscale modelling in the Alpilles experiment in France. EGS 2002, 27. General assembly, Nice (FR), 21-26 Apr 2002. Geophys. Res. Abstr. (CD-ROM) (2002) 4. See abstract and poster

Hasager, C.B., Olioso, A., Jacob, F. 2002b Scaling surface heat flux from eddy correlation data to NOAA AVHRR resolution with a microscale flux aggregation model for the Alpilles experiment in France. In: Proceedings on Workshop on Remote Sensing in Hydrology, Montpellier, 2-5 October 2001 France (in press)

Hulme, M., D. Conway, P.D. Jones, T. Jiang, X. Zhou, E.M. Barrow, and C. Turner, 1995: Construction of a 1961-1990 European climatology for climate change modelling and impact applications. Int. J. Climatol., 15, 1333-1363.

Huang, X-Y, Yang, X., Gustafsson, N., Mogensen, K.S. and Lindskog, M., 2002. HIRLAM 4DVAR. Hirlam Newsletter No. 41, 45-50. Available from SMHI, Norrkøbing, Sweden.

IGBP, 1998, The terrestrial carbon cycle: Implications for the Kyoto Protocal, *Science*, vol 280, 1393-1394

Jensen, N.O. and C.B. Hasager 2000 Scaling up evaporation from field to regional estimates. EGS 2000, 25. General assembly: Millennium conference on earth, planetary and solar systems sciences, Nice (FR), 25-29 Apr 2000. *Geophys. Res. Abstr.* (CD-ROM) (2000) 2 (http://www.copernicus.org/EGS/egsga/nice00/programme/abstracts/aac6249.pdf)

Jensen, N.O., Hasager, C.B. and Larsen, S.E. 2002 Aggregation of momentum and temperature roughnesses based on satellite data. European Geophysical Society 2002, XXVII General Assembly, Nice, France, 21-26 April, *Geophys. Research. Abstracts.* (CD-ROM) See abstract

Jensen N.O. and P. Hummelshøj (1995) Derivation of canopy resistance for water vapour fluxes over a spruce forest, using a new technique for the viscous sublayer resistance. *Agri. and Forest Met*., **73**, 339-352.

Jensen N.O. and P. Hummelshøj (1997) Erratum to "Derivation of canopy resistance for water vapour fluxes over a spruce forest, using a new technique for the viscous sublayer resistance". *Agri. and Forest Met.*, **85**, 289.

Kaimal, J.C. and Finnigan, J.J. 1994 *Atmospheric Boundary Layer Flows. Their structure and measurement.* Oxford University Press, Oxford, 1-289

Kidder S.Q. and T.H.V.Haar, 1995, Satellite Meteorology. An introduction, Academic Press, San Diego, USA, pp466

Machenhauer B., M. Windelband, M. Botzet, J.H. Christensen, M. Déqué, R.G. Jones, P.M. Ruti and G. Visconti, (RACCS) 1998: Validation and analysis of regional present-day climate and climate simulations over Europe. MPI Report No. 275, Max-Planck-Institute, Hamburg.

Mason, P.: 1988, 'The Formation Of Areally-Averaged Roughness Lengths', *Quarterly Journal of the Royal Meteorological Society* **114**, 399-420

Mõlder, M., Sugita, M., Hiyama, T., and Bergstrom, H.: 1998, 'Regional Sensible Heat Flux and Thermal Roughness Length of an Inhomogeneous Landscape', *Hydrological Processes* 2115-2131

National Cadastre and Survey (1995-2000), Top10DK digital vector map. Denmark

Navascues, B. Rodrigues, E. and Ayuso J. J., 2002. The new HIRLAM surface analysis. Proceedings of the SRNWP/HIRLAM Workshop on Surface Processes. Turbulence and Mountain Effects. INM, Madrid 22-24 October 2001, 37-44.

Price, J. C., 1984, Land surface temperature measurements from the split window channels of the NOAA advanced very high resolution radiometer. Journal of Geophysical Research, 89, 7231-7237.

Prince, S. D., Goetz, S. J., Dubayah, R. O., Czajkowski, K. P. and Thawley, M. (1998). Inference of surface and air temperature, atmospheric precipitable water and vapor pressure deficit using AVHRR satellite observations: comparison with field observations. Journal of Hydrology 212-213: 231-250.

Rodrigues, E. Navascues, B. and Ayuso, J .J., 2002. The tiling surface scheme for HIRLAM: features and latest results. Proceedings of the SRNWP/HIRLAM Workshop on Surface Processes. Turbulence and Mountain Effects. INM, Madrid 22-24 October 2001, 55-63.

Roeckner et al., 1996: The atmospheric general circulation model ECHAM-4: model description and simulation of present-day climate. MPI Report No. 218, Max-Planck-Institute, Hamburg.

Sass, B.H., 1994: The DMI Operational HIRLAM Forecasting System Version 2.3 - A Short Summary: DMI Technical Report 94-8.

Sass, B.H. and J.H. Christensen, 1995: A simple framework for testing the quality of atmospheric limited-area models. Mon. Wea. Rev., **123**, 444-458.

Sass, B.H., Nielsen, N.W., Jørgensen, J.U., Amstrup, B.,Kmit, M. 1999 The operational DMI-HIRLAM. Danish meteorological Institute, Copenhagen, Technical report 00-26. 51 pp.

Schmid, H. P. and Bünzli, B.: 1995, 'The Influence Of Surface Texture On The Effective Roughness Length', *Quarterly Journal of the Royal Meteorological Society* **121**, 1-21

Schüssel, P., Schanz, L., and Englisch, G., 1995, Retrieval of latent heat flux and longwave irradiance at the sea surface from SSM/I and AVHRR measurements. Advanced Space Research, 16(10), 107-116.

Sellers P.J., D.A.Randall, G.J.Collatz, J.A.Berry, C.B.Field, D.A.Dazlich, C.Zhang, G.D.Collelo and L.Bounoua, 1996, A revised land surface parameterization (SiB2) for atmospheric GCMs. Part I. Model formulation., *J.Climate* Vol 9, no 4, p676-705

Soegaard, H., Madsen, S.N. and Hasager, C.B. (1998b): Estimation of aerodynamic roughness and soil moisture in agricultural areas using SAR data. Project AO2.DK104, Final Report, Institute of Geography.

Soegaard, H., Nielsen, N.W., Christensen, J.H., Rasmussen, M.S., Hasager, C.B., Boegh, E., Jensen, N.O. 2002 Optimizingh high resolution local area meteoroligcal models by remotely sensed surface boundary conditions (in prep.)

Stewart J.B., E.T.Engman, R.A.Feddes and Y.Kerr (eds.), 1996, Scaling up in hydrology using Remote sensing, John Wiley and Sons, Chistester, UK, pp255

Stull, R. B.: 1991, *An Introduction to Boundary Layer Meteorology*, Kluwer Academic Publishers, Dordrecht, 1-666

Tanré, D., Deroo, C., Duhaut, P., Herman, M., Morcrette, J. J., Perbos, J., and Deschamps, P. Y. (1987). Simulation of the Satellite Signal in the Solar Spectrum (5S). User's guide. Laboratoire d'Optique Atmospherique, Université des Sciences et Techniques de Lille, France.

Valiente, J. A., Nunez, M., Lopez-Baeza, E. and Moreno, J. F. 1995 Narrow-band to broad-band conversion for Meteosat-visible channel and broad-band albedo using both AVHRR-1 and –2 channels. *Int. J. rem. Sens.* **16(6)**: 1147-1166

Viterbo, P., 1996, The representation of surface processes in general circulation models, European Centre for Medium-Range Weather Forecasts, Reading, UK, pp201

Wood N. and P.Mason, 1991. The influence of static stability on the effective roughness lengths for momentum and heat transfer, Q.J.R.Meteorol.Soc.117, 1025-1056

Appendix I

Publications from the SAT-MAP-CLIMATE project

The publications highlighted in **bold** are refereed publications.

Boegh, E., Soegaard, H., Christensen, J.H., Hasager, C.B., Jensen, N.O., Nielsen, N.W., Rasmussen, M.S. 2002 Combining weather predictions and remote sensing data for the calculation of evapotranspiration rates in Denmark. *Int. J. Remote Sensing* (submitted, June 2002)

- Boegh, E., Soegard, H., Christensen, J.H., Hasager, C.B., Jensen, N.O.; Nielsen, NW., Rasmussen, M.S. 2002 The use of HIRLAM climate predictions and AVHRR data for the calculation of evapotranspiration rates in Denmark. *First International Symposium on Recent Advances in Quantitative Remote Sensing*, 16-20 September 2002, Valencia, Spain. (proceedings paper submitted)

- Hasager, C.B., 2001. The SAT-MAP CLIMATE project. DSAR (Danish Society on Atmospheric Research) Annual Meeting, Copenhagen (DK), 15 Nov 2001. (abstract).

- Hasager, C.B., 2002 Microscale surface flux aggregation in heterogeneous terrain using remote sensing data. In: *Proceedings. International workshop on landscape heterogeneity and aerodynamic roughness: Modelling and remote sensing perspectives*, Antwerp (BE), 12 Oct 2001. Debie, H.; Ridder, K. De (eds.), TAP/R/05 (2002) p. 14-18

- Hasager, C.B., Jensen, N.O., Satellite based bio-geophysical parameter mapping and aggregation modelling for weather prediction and climate models. International Geoscience and Remote Sensing Symposium *IGARSS 2000 Symposium,* Honolulu, HI (USA), 24-28 Jul 2000. See abstract

- **Hasager, C.B., Jensen, N.O., Boegh, E., Soegaard, H., Schelde, K. & Thomsen, A., 2001. Scaling-up evapotranspiration from field to regional scale based on optical remote sensing scenes. In the *Proceedings of symposium Remote Sensing and Hydrology 2000*, Santa Fe, New Mexico, USA, April 2000. IAHS Publ. No. 267, 292-295. See abstract**

- Hasager, C.B.; Nielsen, N.W.; Christensen, J.H.; Søgaard, H.; Bøgh, E.; Rasmussen, M.S.; Jensen, N.O., 2001 Satellite-based albedo, sea surface temperature and effective land roughness maps used in the HIRLAM model for weather and climate scenarios. American Geophysical Union (AGU) Fall Meeting, San Francisco, CA (US), 10-14 Dec 2001. *Eos Trans. Am. Geophys. Union Suppl.* (2001) **82** (no.47), F206, See abstract and poster

- **Hasager, C.B. Nielsen, N.W., Jensen, N.O., Christensen, J.H, Dellwik, E. Soegaard, H. and Boegh, E. 2002 Effective roughness calculated from satellite-derived land cover maps and hedge information and used in a weather forecasting model. *Boundary-Layer Meteorology* (submitted, June 2002)**

- Hasager, C.B., Soegaard, H., Nielsen, N.W., Christensen, J.H., Boegh, E., Jensen, N.O. 2002 Aggregation of satellite remote sensing-based land cover roughness applied to meteorological modelling. *34th COSPAR Assembly Scientific (Committee on Space Research). The Second World SpaceCongress*. Houston, Texas, USA, 10-19 October 2002. (abstract submitted)

- Jensen, N.O. and C.B.Hasager, 1999 Surface heat flux averaging in heterogeneous terrain, IUGG 99, Birmingham, UK, 18-30 July 1999 (abstract)

- Jensen, N.O. and C.B. Hasager 2000 Scaling up evaporation from field to regional estimates. European Geophysical Society (EGS). 25. General Assembly: Millennium conference on earth, planetary and solar systems sciences, Nice (FR), 25-29 Apr 2000. *Geophys. Research. Abstr.* (CD-ROM) (2000) 2. See abstract

- Jensen, N.O., Hasager, C.B. and Larsen, S.E. 2002 Aggregation of momentum and temperature roughnesses based on satellite data. European Geophysical Society 2002, XXVII General Assembly, Nice, France, 21-26 April, *Geophys. Research Abstracts.* (CD-ROM). See abstract

- Jensen, N.O., Hasager, C.B., Nielsen, N.W., Christensen, J.H., Soegaard, H., Boegh, E. 2002 Satellitbilleder og vejrprognoser. Nordic Meteorological Meeting (Nordisk Meteorolog Møde). Copenhagen 27-31 May 2002. See abstract and slide show

- Nielsen, N.W., Hasager, C.B., Soegaard, H., Christensen, J.H., Jensen, N.O., Boegh, E., 2002 Results of the SAT-MAP-CLIMATE project. *HIRLAM Newsletter,* **No. 41**. p. 74-78 Available from SMHI, Norrkoebing, Sweden

- Nielsen, N.W. SAT-MAP-CLIMATE: A pilot project about use in NWP of surface parameters derived from satellite measurements. *HIRLAM ASM,* Copenhagen, Denmark, 4 April 2002

- **Soegaard, H., Nielsen, N.W., Christensen, J.H., Rasmussen, M.S., Hasager, C.B., Boegh, E., Jensen, N.O. 2002 Optimizingh high resolution local area meteoroligcal models by remotely sensed surface boundary conditions (in prep.)**

- Soegaard, H., C.B.Hasager, N.Woetmann, J.H.Christensen, N.O.Jensen, E.Boegh and M.S.Rasmussen 2000 Combining satellite data and a high resolution meteorological model for estimation of surface fluxes and resistances. European Geophysical Society, 25. General assembly: Millennium Conference on Earth, Planetary and Solar Systems Sciences, Nice (FR), 25-29 Apr 2000. *Geophys. Research Abstr.* (CD-ROM) (2000) 2. See abstract

Spin-off publications

- Boegh, E. and Soegaard, H. 2002. Remote sensing based estimation of evapotranspiration rates. *International Journal of Remote Sensing*, (submitted)

- Hasager, C.B.; Olioso, A.; Jacob, F. 2002 Parametrisation of aggregated roughness and sensible heat flux from field scale to hydrological scale by microscale modelling in the Alpilles experiment in France. EGS 2002, 27. General assembly, Nice (FR), 21-26 Apr 2002. *Geophys. Research Abstr.* (CD-ROM) (2002) 4. See abstract and poster

- Hasager, C.B., Olioso, A., Jacob, F. 2002 Scaling surface heat flux from eddy correlation data to NOAA AVHRR resolution with a microscale flux aggregation model for the Alpilles experiment in France. *In: Proceedings on Workshop on Remote Sensing in Hydrology,* Montpellier, 2-5 October 2001 France (in press)

- Olioso, A.; Jacob, F.; Hadjar, D.; Lecharpentier, P.; Hasager, C.B., 2002 Spatial distribution of evapotranspiration and aerodynamic roughness from optical remote sensing. *In: Proceedings of International Workshop on Landscape Heterogeneity and Aerodynamic Roughness: Modelling and Remote Sensing Perspectives*, Antwerp (BE), 12 Oct 2001. Debie, H.; Ridder, K. De (eds.), TAP/R/05 (2002) p. 19-26

Appendix II

On the microscale aggregation software

The first and second version of the microscale aggregation programme is graphed in Figure 6-6 and Figure 6-7, respectively. The first version is programmed by Helmut Frank (now at DWD). The new features are programmed by Jens V. Olsen (Risø). The programme is in Visual Fortran and runs on pc.

In the following the items in the sketch are underlined

INPUT

Maps derived from satellites (define number of cells and domain size. File format IEEE32)

- Surface temperature in Celcius (Surface temp.)
- Land cover classes with numbers (Land cover)
- Leaf area index map (*LAI*)

Meteorological observations (from mast, radiosounding or mesoscale model)

- Wind speed vector in m s^{-1} as u_x v_y components. Example (5 0) is 5 m s^{-1} towards the East at the computationel level (*U*)
- Air temperature in Celcius at the computational level (*Ta*)
- The computational level z_r.

INDECES

- List of assignment values of local z_0 per land cover class number (Index z0)
- List of index numbers for z_{0t} with translation from land cover class to z_{0t}-type (Index No.)
- Ratio value between z_0/z_b for initialization of the z_{0t}-map (r) (OBS. Not shown in Figure 6-7. Always used in Figure 6-6)
- Ix-formula for z_{0t} (eqs. 6.23-6.26)
- The water roughness is initialized with a z_0 value

MODEL DESCRIPTION

The initial model run starts with three maps: "Surface temp.", "z_0" and "z_{0t}" and values of the wind vector (U) and air temperature (Ta) at the computational level. The map of "u_*" is set to 0.4 m s^{-1} in the initial run and the initial map of "z_{0t}" is set as a ratio of "z_0".

After one iteration the new values of "u_*" will feed into the "ix formulaes" and the "Water only" formula (2-dim arrays) and thereby generate a new set of "z_0" and "z_{0t}" maps.

When the model converges the final maps of "u_*" and "2_*" are calculated.

OUTPUT

Based on the "u_*" and "2_*" maps the heat flux map "H" is calculated.
The outputs are named ustper.db, Tstper.db and Hper.db, respectively (file format IEEE32).
New outputs of the calculated "z_0" and "z_{0t}" maps are made.
Further is the effective area average of "$<z_0>$" and "$<z_{0t}>$" among other values output in a text-file or on screen.

OTHER FEATURES

Generate synthetic data of "Surface temp.", "z_0" and "LAI"maps by input of T_{s1} T_{s2}, z_{01} z_{02}, LAI_1, LAI_2 values in checkerboard pattern instead of filenames for the maps. Change land cover types in the foulum.csv for index-file.
Decide on the ratio r between "z_0"/ "z_{0t}", e.g. 0.1, 0.01 and 0.001.
Use file flowz0T_map.i for input variables.

Bibliographic Data Sheet **Risø-R-1350(EN)**

Title and authors

SAT-MAP-CLIMATE Project Results

Charlotte Bay Hasager, Niels Woetmann Nielsen, Henrik Soegaard, Eva Boegh, Jens Hesselbjerg Christensen, Niels Otto Jensen, Michael Schultz Rasmussen, Poul Astrup and Ebba Dellwik

ISBN	ISSN
87-550-3079-3 87-550-3080-7 (Internet)	0106-2840

Department or group	Date
Wind Energy Department Atmospheric Physics Programme	August 2002

Groups own reg. number(s)	Project/contract No(s)
	Sagsnr. 5006-00-0063

Sponsorship

Danish Research Agency, ESA-følgeforskning (Space Research)

Pages	Tables	Illustrations	References
71	10	24	63

Abstract (max. 2000 characters)

Earth Observation (EO) data from imaging satellites are analysed with respect to albedo, land and sea surface temperatures, land cover types and vegetation parameters such as the Normalized Difference Vegetation Index (NDVI) and the leaf area index (LAI). The observed parameters are used in the DMI-HIRLAM-D05 weather prediction model in order to improve the forecasting. The effect of introducing actual sea surface temperatures from NOAA AVHHR compared to climatological mean values, shows a more pronounced land-sea breeze effect which is also observable in field observations. The albedo maps from NOAA AVHRR are rather similar to the climatological mean values so for the HIRLAM model this is insignicant, yet most likely of some importance in the HIRHAM regional climate model. Land cover type maps are assigned local roughness values determined from meteorological field observations. Only maps with a spatial resolution around 25 m can adequately map the roughness variations of the typical patch size distribution in Denmark. A roughness map covering Denmark is aggregated (ie area-average non-linearly) by a microscale aggregation model that takes the non-linear turbulent responses of each roughness step change between patches in an arbitrary pattern into account. The effective roughnesses are calculated into a 15 km by 15 km grid for the HIRLAM model. The effect of hedgerows is included as an added roughness effect as a function of hedge density mapped from a digital vector map. Introducing the new effective roughness maps into the HIRLAM model appears to remedy on the seasonal wind speed bias over land and sea in spring. A new parameterisation on the effective roughness for scalar surface fluxes is developed and tested on synthetic data. Further is a method for the estimation the evapotranspiration from albedo, surface temperatures and NDVI succesfully compared to field observations. The HIRLAM predictions of water vapour at 12 GMT are used for atmospheric correction of the satellite parameters derived in the afternoon.

Descriptors INIS/EDB

CLIMATE MODELS; DATA ANALYSIS; EVAPORATION; FORECASTING; ROUGHNESS; SATELLITES; TRANSPIRATION; VERIFICATION; WEATHER